Surface Engineering of MXene-Based Materials for Next-Generation Rechargeable Batteries

Shahid Ashraf[1], Amna Abrar[2], MD Mahbub Alam[3], Muhammad Hisham Al Nasir[4], Maneeb Ur Rehman[5], Jehanzad Zafar[6], Muhammad Talha Saeed[7], Muhammad Waqas[8], Shoaib Akmal[9], Sajid Khan[10], Shah Wali Ullah[11]

[1]*Department of Physics, University of Agriculture Faisalabad, Pakistan*
[2]*Department of Chemistry, School of Science, Tianjin Key Laboratory of Molecular Optoelectronic Science, Tianjin University, China*
[3]*Department of Mechanical Engineering, Key Laboratory of Advanced Ceramics and Machining Technology of Ministry of Education, Tianjin University, China*
[4]*Department of Physics, Riphah International University, Pakistan*
[5]*Faculty of Basic and Applied Sciences (FBAS), International Islamic University (IIU), Pakistan*
[6]*Department of Material Science and Engineering, Xi'an Jiaotong University, China*
[7]*Institute of Chemical Sciences, Gomal University Dera Ismail Khan, Pakistan*
[8]*Department of Solid State Physics, University of the Punjab, Pakistan*
[9]*Department of Physics, The University of Lahore (UOL 1-km Defence Road, Pakistan.*
[10]*Department of Mechanical Engineering Technology, The Benazir Bhutto Shaheed University of Technology & Skill Development, Pakistan.*
[11]*Advanced Functional Materials (AFM) Laboratory, Engineering Physics Department, Institute Technology Bandung, Indonesia.*
Email: shahid.ashraf97@yahoo.com

Abstract: Next-generation rechargeable batteries are being developed to address challenges such as low cost, high stability, high energy density, and safe energy storage materials. MXene-based mate-rials have attracted wide attention due to their unique properties, large surface area, high electrical conductivity, and easy dispersion in solvents compared to graphene. MXene derived from carbide and nitrides of transition metals (Ti3C2TX) have unique properties compared to other two-dimensional materials (2D) for use in rechargeable batteries. MXene electrodes delivered excellent performance and cyclic stability in various rechargeable secondary batteries. This re-view highlights the role of MXene in next-generation rechargeable batteries of lithium ion bat-teries (LIBs), lithium sulfur batteries (LISBs), sodium ion batteries (SIBs), zinc ion batteries (ZIBs), aluminium ion batteries (AlIBs), potassium ion batteries (PIBs) and magnesium ion bat-teries (MIBs). Moreover, in this review, we discussed the current research developments to im-prove the efficiency of energy storage devices and present the future research direction to im-prove the scalability, stability, and overall performance of MXene-coated electrodes in recharge-able batteries to overcome the energy storage challenges.

Keywords: MXenes, Rechargeable Batteries, Energy Storage Devices, Structure Design.

1. Introduction

In modern days, renewable energy resources are being discussed widely as environment-friendly energy use. Moreover, the output of renewable energy resources is weather and climate dependent [1]. Due to the intermittent nature of renewable energy resources, Energy storage devices ensure a continuous and reliable energy supply. Renewable energy storage technology is widely being explored by researchers due to advancements in portable electronic devices, battery electric cars, and hybrid electric vehicles [2]. Metal air batteries will be in high demand batteries in the future due to their variety of applications

in battery electric cars, hybrid electric vehicles, and grid energy storage due to their high power, open structure, and high energy density. Rechargeable batteries have a huge demand due to their high efficiency, long life cycle, low cost, cheap maintenance, and diverse range of power densities and energies [3]. However, researcher focused on two-dimensional (2D) materials to develop next-generation rechargeable batteries because of their integration in an array of energy generation and energy storage applications. Electrode materials play a crucial role in rechargeable batteries, and many materials have been developed as electrode materials. However, maximum energy storage can be achieved in high power density materials, where electrons and ions can move rapidly [4]. Only open 2D materials have excellent storage capacity due to their large specific surface area and capability to facilitate ion transportation, while other 2D materials cannot meet the requirements of life cycle, power density, and energy density. Graphene has high mechanical strength and electrical conductivity, but it shows limited charge storage capacity due to charge storage on its surface only. Transition metal dichalcogenides (TMDs) show high initial capacities, but their poor capacity and low electrical conductivity remain significant challenges [5]. Lithium ion batteries are considered as most commonly energy storage devices due to their remarkable cyclic stability and energy density, but limited resources of lithium, toxic organic electrolytes, unsafe and high cost promoted the development of reliable, low cost and safe energy storage devices [6]. In the past decade, multivalent metal ion batteries, including calcium (Ca), magnesium (Mg), zinc (Zn), and aluminium (Al), rapidly developed due to their high charge transfer, low cost, high safety, and abundant natural reserves [7,8]. To overcome these issues, MXene is a new material resulting from graphene that can be used to overcome these issues. MXene is the result of long-term research on two-dimensional materials extending to metal oxides, transition metal dichalcogenides, metal oxides, and so on [8]. MXene is a family of two-dimensional materials that have a composition of carbides and transition metal nitrides with randomly distributed surface functional groups. MXene earned a title of "next-wonder material" in a very short time [9]. MXene carries unique properties as compared to graphene, being energy storage material with a large surface area [10], easy dispersion of solvents [11], rich surface chemistry [12], and high electrical conductivity 2×10^{-5} Sm^{-1} [13]. These properties of MXene include a two-dimensional structure to facilitate the rapid transportation of ions and mechanical flexibility at the nanosheet level. Next generation rechargeable batteries demand to improve the electrochemical performance including long-term stability, high power density and high energy which depends upon the properties of electrode materials [14]. The idea of MXene synthesis was replaced from single transition metal toward double transition metal-based MXene, and fabrication techniques were replaced by stamping/printing strategies for scaling up for standardized mass production. Researchers lifted off the limitations on the fabrication of electrodes with challenging designs to explore the scope of MXene in energy storage applications [15]. Hussain et al.. explored the significance of electrode designing and surface engineering with nanostructure morphology [16]. MXene-based electrodes can be developed by combining MXene with other materials [17]. Almost 30 MXene electrodes have been experimentally reported, and the performance of $Ti_3C_2T_X$ attracted more attention among all because it offers high volumetric capacitance due to the redox-active titanium atom. Controlled composition of surface terminations and metal/carbon ratio on surface MXene not only improves the energy storage and electrochemical performance but also avoid stacking of MXene single layers [18]. In this review, we discussed the role of MXene in next-generation rechargeable batteries and summarized the performance of MXene in rechargeable batteries.

2. Overview of MXene Materials and their Unique Properties

For more than a decade, Tremendous research on the exfoliation of graphene has attracted the great attention of scientists to improve the efficiency of conventional devices, e.g., solar steam production, rechargeable lithium ion batteries, photodetectors, fuel production, and photothermal therapies. Derivatives of Phosphorene, MoS_2, proved to be efficient materials among 2D materials. After the successful preparation of graphene in 2004, 2D materials attracted wide attention due to their mechanical and physiochemical properties [19]. At First time, In 2011, Prof. Yury and Prof. Michael W. Basrsoum developed MXenes (Ti_3C_2Tx) derived from carbide and nitrides of transition metals, but due to the use of hazardous hydrofluoric acid in synthesis methods, they still remain under investigation by researchers [20]. MXene have $M_{n+1}AX_nT_x$ chemical composition where n=1,2 or 3 Where M is transition metal (Cr, Ti, V, Zr, Nb, Hf, Mo) A is element of group A or semiconductor and X is Carbon or nitride while T stands for surface termination group (O, OH, F) [Figure 1] [21].

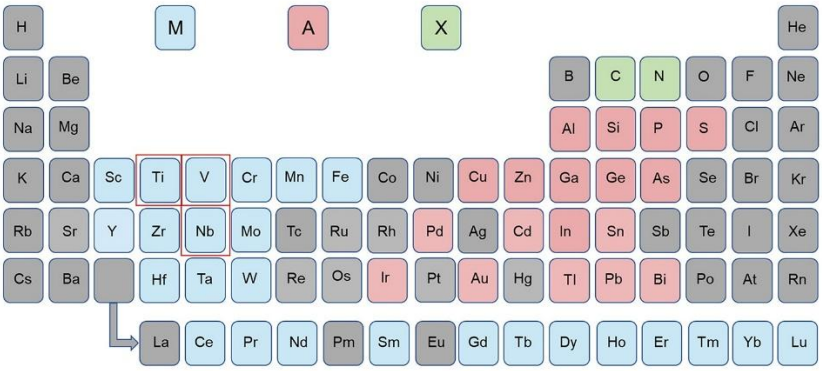

Fig.1 Illustrate the fragments of the periodic table classified as M, A, and X in MAX phases [22]

MXenes are widely used in future applications such as Sensors, gas adsorption, photocatalysis, Water purification, and Energy storage [23] due to their various physical and chemical characteristics e.g. superior conductivity (3550±100 S/cm for V_2CTx) high hydrophilicity (contact angle 21.5º-35.0º), tunable interlayer distance and good mechanical properties [7]. MXenes are highlighted as potential host material for lithium ion batteries (LiB) because MXenes relieve the volume size of the electrode, enhance the electronic conductivity, diffusion kinetics of large size ions in electrodes suppress the dendrite growth, uniform plating and impeding the "shuttle effect" of soluble species [24]. MXenes have high electrochemical activity, a high young's modulus, functionalized surface, large surface area, and low transportation energy barrier resulting in excellent flexibility, superior physiochemical properties, and high thermal and electronic conductivity. Until now, almost 100 MXenes have been predicted theoretically and 30 MXenes prepared by experimental techniques, which are useful for numerous applications. The electrochemical energy storage efficiency of MXenes is directly related to their structural, electronic, and chemical properties [25].

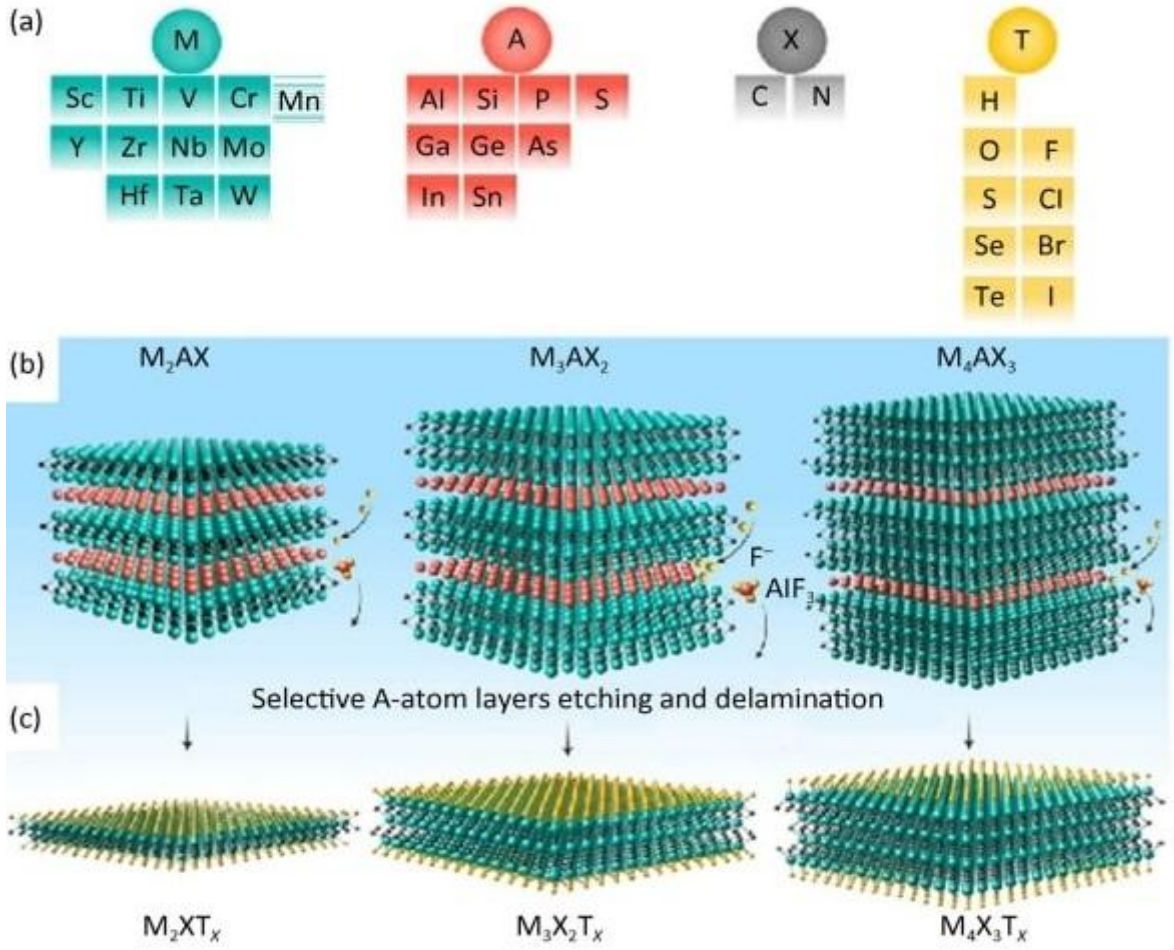

Fig.2a Derived pristine MXene nanosheet and Structures of Max phases. Fig.2b Schematic MAX phases crystal structure of M_2AX, M_3AX_2, and M_4AX_3. Red atoms represent a layer of A group that

will be removed by the etching methodology. C) Illustrate the schematic representation of obtained MXene after the etching process. Surface Terminations T is denoted by yellow atoms.

Fig.2a represents that MXene essentially obtained from $M_{n+1}AX_n$, which is MAX precursor. As today MXene family include $(Ti_{0.5}, Nb_{0.5})_2C$, Ti_2C, Ti_3C_2, V_2C, Ti_3CN, Ta_4C_3 and $(V_{0.5}, Cr_{0.5})$. Fig.2 b-c $M_{n+1}AXn$ phases value of changes from 1 to 3, and single MXene sheets of M_2X consist of 3 atomic layers, M_3X_3 consist of 5 atomic layers, and M_4X_3 consist of 7 atomic layers [26].

In all phases, MXene layer thickness is less than 1 nm, and lateral dimensions reach up to tens of microns [27]. M_2X, M atoms have a hexagonal closed-packed structure, while in M_3X_2 and M_4X_3, M atoms have a centred cubic structure.

2.1 Significance of MXenes for next-generation rechargeable batteries

In the past decade, the consumption of fossil fuels was widely discussed to overcome the energy crisis. As a result, various renewable energy sources, including solar cells, wind energy, and tidal energy, have been discussed. Meanwhile, efficient energy storage materials are required on an urgent basis to store electrochemical energy via electrochemical energy storage devices (EEDS). In this regards, various rechargeable low-cost batteries based on metal ion electrode batteries e.g. aluminium, sodium, magnesium, potassium metal electrodes batteries have been developed and showing similar potential as LiB addressing the energy storage challenges, and specific role of MXene nanosheets as conductive additive, current collector, and two-dimensional support of hybrid materials are summarized in Figure.3 [28].

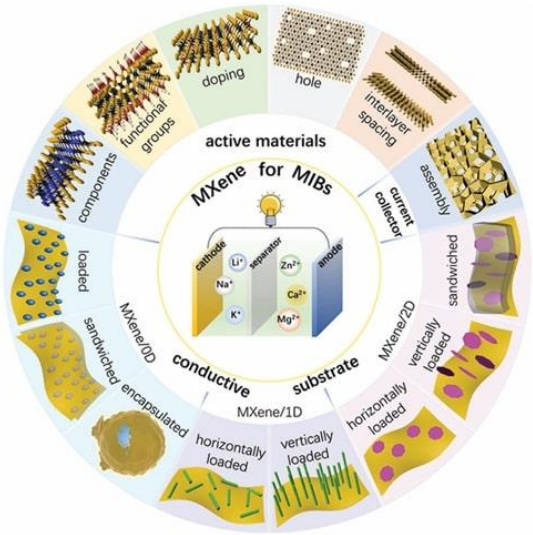

Fig.3 Schematic representation of MXene-based nanostructure metal ion batteries [29]

MXenes possess competitive chemical and structural properties than other 2D materials for secondary batteries. The electrochemical properties of MXenes increased by combining with other nanomaterials due to the synergistic effect. It's crucial to mention that the cyclic stability and metal ion capacity of modified MXenes are far better than the bare MXenes during charging and discharging [30]. MXene catches the high attention of researchers due to its high electrical conductivity, which plays a significant role in enhancing the transference of ions and electrons. The $Ti_3C_2T_X$ shows electrical conductivity of approximately 9880 S cm^{-1} with 88 nm thinfilm thickness. Improving the electrochemical performance of MXene (e.g., energy density, capacity, capacitance, and cyclic stability) of devices has attracted wide attention to the properties of MXene-based electrodes (e.g., restacking, surface termination, and electrical conductivity). Lithium ion batteries (LIBs), sodium ion batteries (SIBs), and lithium sulphur batteries (LISBs) are major devices where MXene electrodes are widely employed. MXene electrodes are widely focused on lithium-ion batteries, although MXene applications are also developing on other secondary batteries, e.g., Zinc, aluminum, sodium, potassium [31], and magnesium ion batteries (ZIBs, AlIBs, SIBs, PIBs, MIBs). MXene can deliver excellent cyclic stability and performance in LIBs due to the low diffusion barrier of lithium ions, low operating voltage (-0.2 to 0.6 V vs Li/Li^+), and high electrical conductivity. Theoretically, MXenes are expected to show higher specific capacity, however, experimental results fall down these predicted values. For example, the specific capacity of V_2CTx as a Lithium ion battery electrode calculated theoretically was high as high as 940 mA hg^{-1} , but the experimentally measured value was just 252 mA h g^{-1}, also, columbic efficiency (CE) was also low. This unsatisfactory performance was due to restacking of MXene nanosheets during synthesis process

and testing and attached terminations on MXene surfaces, which consume Li ions part, resulting into low CE [32].

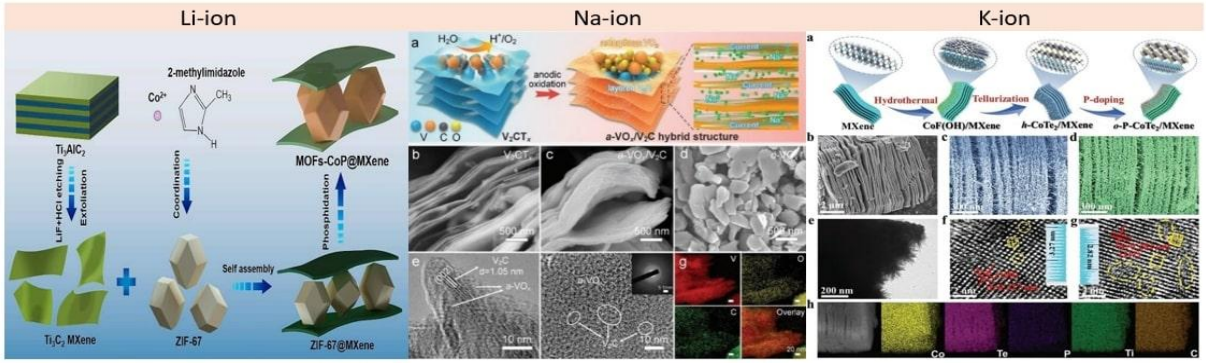

Fig.4 MXene-based composite for a) Lithium ion batteries b) Sodium ion batteries c) Potassium ion batteries Ref a. [167] b.164 c. [33]

Table 1 discusses the performances of MXene-based materials in LIBs, NIBs, and KIBs. [201]

Battery type	Material	Specific capacity ($mAh \cdot g^{-1}$)	Ref.
	Ti_3C	123.6 mAh g^{-1}@ 1C	184
	V_2CT_X	260 mAh g^{-1} @ 1C	34
	Fe_3O_4@ $Ti_3C_2T_X$	747.4 mAh g^{-1} @ 1C	34
	$Ti_3C_2T_X/NiCo_2O_4$	1330 mAh g^{-1} @ 0.1C	35
Lithium	$rGO/Ti_3C_2T_X$	221 mAh g^{-1} @ 50	34
	$SnS/Ti_3C_2T_X$	412.8 mAh g^{-1} @ 100	36
	$MoS_2/Ti_3C_2T_X$	656 mAh g^{-1} @ 50	37
	Nb_2CT_X/CNT	170 mAh g^{-1} @ 1C	37
	$Hf_3C_2T_X$	90 mAh g^{-1} @ 10 mAg− 1	38
	V_2CTx	22 mAh g^{-1} @ 20C	39
Na-ion	$Ti_3C_2T_X/FeS$	563mAhg-1@0.1 Ag^{-1}	40
Battery	$Ti_3C_2T_X/VO_2$	280.9mAhg^{-1}@0.1 Ag^{-1}	
	$Ti_3C_2T_X/Sb_2O_3$	472mAhg^{-1}@0.1 Ag^{-1}	
	$Ti_3C_2T_X/TiO_2$	153mAhg^{-1}@0.6 Ag^{-1}	
	Ti_3CNTx	90mAhg^{-1}@0.01 Ag^{-1}	
	MoSe2/MXene@C	350mAhg^{-1}@0.1 Ag^{-1}	
	$Ti_3C_2T_X/MoS_2$	290.7mAhg^{-1}@0.05 Ag^{-1}	
	Ti_3C_2-Derived	105mAhg^{-1}@0.1 Ag^{-1}	
K-ion Battery	Potassium Titanate NRs		

Lithium sulphur (Li-S) has a 5-fold energy density. Li-S battery is considered a promising candidate to store energy for commercial applications beyond the current LiBs. Li-S has numerous advantages due to its theoretical energy density (2600Wh kg^{-1}) and theoretical specific capacity (1675 $mAhg^{-1}$). A Major limitation in Li-S batteries is the dissolution of polysulfide in electrolytes results in lithium polysulfide (LPS). To overcome this challenge, various materials, including multiwall carbon nanotubes and polyaniline nanofibers (e.g., MoS_2/CNT, $MgBO_2(OH)$/CNT, PANiNF/MWCNT), are developed, which behave as functional separators. Nuo Li et al.. applied an ultralightweight modified separator on the Li-S battery consisting of Ti_3C_2Tx/CNTs 10%PP (Polypropylene) with 0.016 mg cm^{-2} mass loading resulted into improve the movement of Lithium ions. Although Li-S batteries have excellent reversible capacity and stability among numerous storage devices [41].

Recently, rechargeable batteries based on 2D anode materials have shown high volumetric and gravimetric energy densities. Single-type layered nanosheets of MXenes, transition metal dichalconides, and Black phosphorous (With M=Ti, Mo, Nb, V, and X=C, N) are experimentally investigated, leading to poor performance and rapid capacity fading. Pomerantseva et al. designed heterostructure 2D materials by merging various 2D materials. Yierpan et al. found that LiBs and sodium ion batteries NIBs have insufficient rate capability and energy density to satisfy customer demands. They thoroughly investigated Li intercalation within the Van Der Waals heterostructure MXenes/Graphene aiming their potential applications in rechargeable batteries, for this propose monolayers of MXenes (M_2C_2X) where M= (Ti, Sc, V and X=OH, O) have discussed, while in experimental investigation by mixing of $Ti_3C_2X_X$ with graphene resulted into highly enhanced mobility of hall carrier and electrical conductance and also found that there are only two stable heterostructure based on graphene (Ti_3C_2Xx + Gr, V_2CO_2+Gr) for Li intercalation based on 1) interlayer separation <0.5 A˚ and inplane lattice parameter <1% 2) Binding

energies of Li atoms surpassing the bilayer graphene 3) Presence of Li atoms in cationic state due to transfer of charge to host material. All the Li absorption sites are in 100% intercalation resulting in an open circuit voltage of 1.49 v for Ti_2CO_2 + Gr and 1.93 v for V_2CO_2+Gr, MXene + Gr have light weight than the bare MXene, which offers superior energy storage density and high electrical conductivity which is crucial for battery operation [42].

In past years, several batteries have attained huge attention, including aluminum-ion batteries, magnesium-ion batteries, sodium-ion batteries, zinc-ion batteries, calcium-ion batteries, and iron-ion batteries. In 2019, the Nobel Prize was awarded to LIBs due to their crucial role in society. However, nowadays, sodium ion batteries have shown large potential in commercial energy storage due to their similar electrochemical process with LIBs and cost-effectiveness [43]. Wang et al reinforced $Ti_3C_2T_X$ monolayer for Na intercalation and suggested that capacity of MXenes materials can be enhance due increasing the interlayer spacing for Na-ion batteries [44]. Yu et al.. applied the first principle of the swarm structure to determine the theoretical capacity of sodium storage for the single atomic layer in 2D material TiC_3. Their results revealed that the 1278 mA.h/g theoretical capacity of TiC_3 for sodium storage which was three times greater than the metal MXenes like Ti_3C_2, Ti_2C which confirms that electrochemical performance of Na ion batteries can be enhanced by increasing the content of carbon within matrix stoichiometry and controlling the thickness of MXene [45]. Naguib et al. present that Ti_3CNT_x as an electrode for K-ion batteries to enhance its storage capacity after observing that K^+ had "pillar effect". Wang et al. designed dendrite free, flexible Zn anode coated by MXene nylon fabric (MXNY) as three-dimensional zinc deposition in situ forming a polydopamine (PDA) as solid electrolyte interface (SEI) resulted into achieve long cyclic stability after 3000 h at current density of 0.5 $mAcm^{-2}$ for 0.5 $mAcm^{-2}$ and achieve 99.6% high columbic efficiency (CE) at current density of 10 $mAcm^{-2}$ for 1$mAhcm^{-2}$ [46].

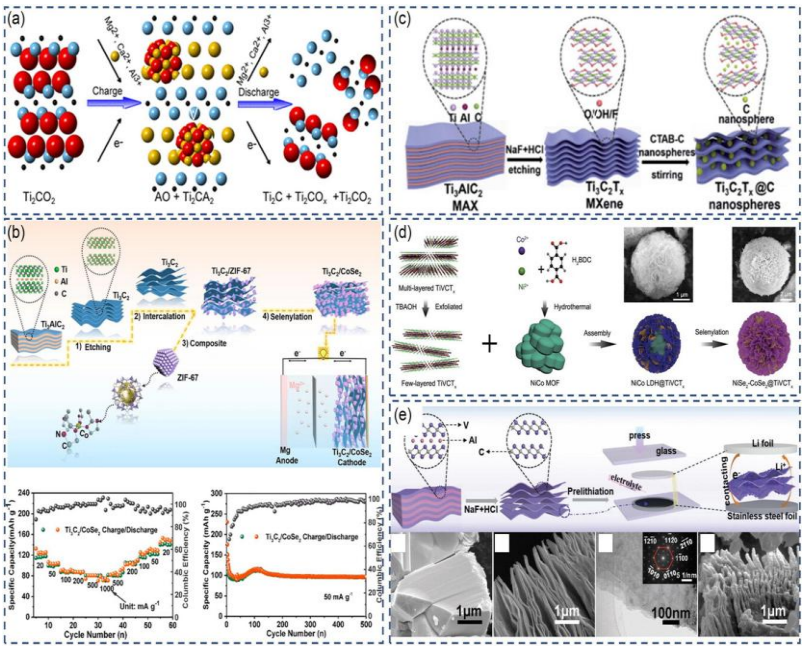

Fig.5 (a) Working mechanism of Na+, K+, Al+3, Mg+2, Ca+2 copy right permission 2014 [222] American chemical society b) Ti3C2/CoSe2 process. Copy right permission [223] 2021, Elsevier c) synthesis of Ti3C2Tx@C nanospheres. Copy right permission [224] 2019, The Royal Society of Chemistry d) synthesis of TiVCTx and NCSe@TiVC heterostructure. Copy right permission [225], 2022, Willey-VCH e) Fabrication of perlihated MXene. Copy right permission [226], 2020, Wiley-VCH

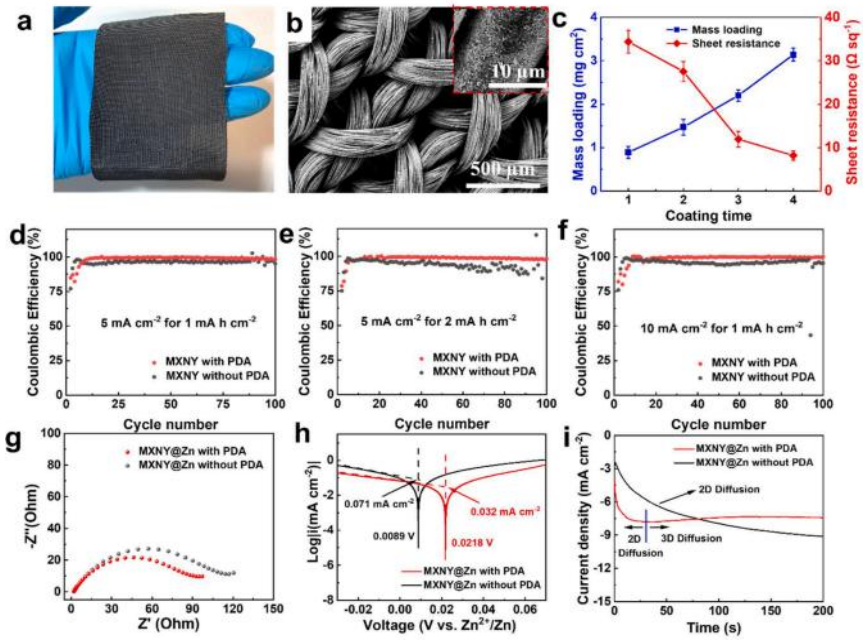

Fig 6. illustrate the coating of MXNY on zinc anode deposition a) digital photograph b) SEM images of MXNY c) Conductivity and mass loading of MXNY as function of coating time d) columbic efficiency (CE) for 1mAgh-1 at 5mAcm-2 e) and 2mAcm-2 f) CE at a current density for 1mAgh-1 at current density of 10mAcm-2 g) electrochemical impedance spectroscopy (EIS) of MXNY@Zn h) linear polarization experiment i) MXNY@Zn with red and black PDA.

Xie et al. [222] reported that MXene based cathode will be highly efficient of MgIBs through experimental and DFT analysis as shown in figure 5a. Liu et al. [223] synthesized $Ti_3C_2/CoSe_2$ by situ salinization as cathode, which shows excellent performance of 75.7 $mAhg^{-1}$ with cyclic stability for MgIBs figure 5b. Fans et al. [47] suggest MXene/Carbon cathode for magnesium ion batteries, which delivered outstanding cyclic stability with a high capacity of 198.7 $mAhg^{-1}$ as in figure 5c. Zhang et al. [48] reported $NiSe_2$-$CoSe_2$@$TiVCT_X$ cathode to investigated the Mg^{+2} storage and resulted into delivered a capacity of 136 $mAhg^{-1}$ after 500 cycle as shown figure 5d. Liu et al. [48] prepared a Li^{+2}/Mg^{+2} hybrid battery using a cathode of prelithiated V_2C as in Figure 5e, which delivered a capacity of 230 $mAhg^{-1}$.

MXNY coated electrode can be prepared by using the dip coating technique. Digital and SEM images in Figure 6a, b show the distribution of MXene on the nylon fabric. Mass loading of MXene 2.2 $mgcm^{-2}$ using 3 times dip coating to reduce the MXNY resistance shown in figure 6c. In blank columbic efficiency of 95.1% for 80 cycles for a capacity of 1 mA h cm^{-2} at a current density of 5mA cm^{-2} shown in figure 6d. After the addition of PDA, 99.4% CE of MXene increased at a current density of 2mA h cm^{-2} for 100 cycles, as shown in figure 6e. Stabilized MXNY CE 99% for 100 cycles with DA electrolyte reaches to 94.8% for 30 cycles with blank electrolye. The current density for 1mA h cm^{-2} reaches up to 10 mA h cm^{-2}, CE 99.6% achieved with PDA SEI, which is better than blank electrolyte as shown in figure 6f. Zinc deposited MXNY tested as electrode to get further insights of PDA SEI on zinc plating and nucleation, ion transportation, symmetric cells and corrosion resistance and EIS with MXNY@Zn with PDA SEI shows lower resistance approximately 105 Ohm than that of MXNY@Zn without PDA SEI which can be attributed to reduce the interfacial side reaction [49].

Various features of MXene, e.g., unique layered structure, fast ion diffusion, low diffusion energy barrier, high electrical conductivity, large number of surface functional groups, and large surface area, enabled the remarkable performance of energy storage devices. These unique features of MXene address the requirements of next-generation rechargeable batteries from LIBs for electric vehicles to emerging alternatives such as Al^+, Mg^+, Zn^+, Na^+, and K^+ batteries, focusing on high safety and low-cost energy storage solutions. Fig. 4a discusses the progress of MXene via in situ growth engineering in rechargeable batteries. While Fig. 4b illustrates the MXene-based rechargeable battery research papers from 2016 to 2024 [50]. The increase in the popularity of electric vehicles enhances the demand for robust power systems. Therefore, the development of MXene-based electrodes is important to enhance the energy storage capacity and cyclic stability for next-generation rechargeable batteries.

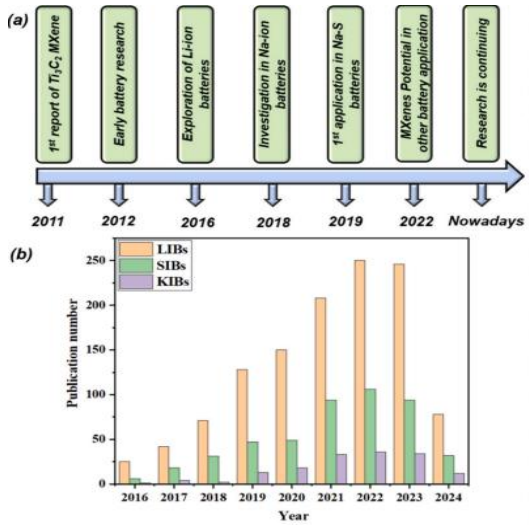

Fig 7. A) Illustrate the advancement in 2D MXene through situ growth engineering from 2011 to 2024 b) Depicts the number of research publications on 2D MXene for the development of Lithium ion, Sodium ion, and potassium ion batteries.

3. Surface Functionalization of MXene

MXene Single layer and multilayer nanostructure can be synthesized using these three methods: 1) chemical transformation, 2) bottom up methods (salt tempered growth and chemical vapor deposition), and 3) top down method (Tailored etching of MAX and non-MAX phases) [51]. Moreover, MXene has poor stability, low mechanical flexibility, and easy restacking, and poor water dispersibility due to the presence of molecular oxygen [52]. Hence, to overcome these challenges, surface functionalization and modification enhance the performance and stability of MXene. Covalent and non-covalent modification used for surface functionalization of pristine MXene. There are three groups of covalent modification [53]: i) those that contain a singe heteroatom [34], ii) those that are surface initiated by macromolecules [54], and iii) those that involve acid halide, alkali metal hydroxide, acid anhydride, organic amines, and epoxy compounds. A combination of electrostatic attraction, hydrogen bonding, and Vander Waals forces give non-covalent surface modification [55].

There are various surface termination groups that enhance the electrochemical charge storage performance. Common types of groups are -OH, -O, and -F, where -OH, -O provide stable thermodynamic performance to batteries, and -F establishes the stable solid electrolyte interphase during the electrochemical reactions in batteries. Xie et al. firstly reported that bare MXene and -O terminated groups can be promising anode material for next-generation rechargeable batteries beyond lithium batteries. Recently, Chen et al. developed Ti_2NS_2 and Ti_2CS_2 as potential anode material for Potassium ion (K-ion) batteries. These sulfurized MXene predicted rapid kinetics and complete adsorption layers for single MXene on both surfaces and shown high theoretical capacity of 381 mA.h/g and 390 mA.h/g respectively [56]. Bao et al. prepared a sulfur-doped MXene (S-$Ti_3C_2T_X$) behave as a cathode in sodium-sulfur batteries (RT Na-S). Sulfur-doped MXene has high surface areas and porous structure, and it contains high loading sulfur up to 4.5 mg/cm^2 and indicates a high capacity of 822 mA.h/g for sodium sulfur batteries while delivering 577 mA.h/g reversible capacity for 500 cylce at 2 C of current rate [57]. Nao et al. suggested F-rich terminations using organic solvents having NH_4HF_2, which dissociate into NH_4F, HF, and other polar solvents. Proposed F-rich $Ti_3C_2T_X$ tested in Na-ion batteries with carbonate electrolytes as anode material which shows double capacity than -O rich terminate [58].

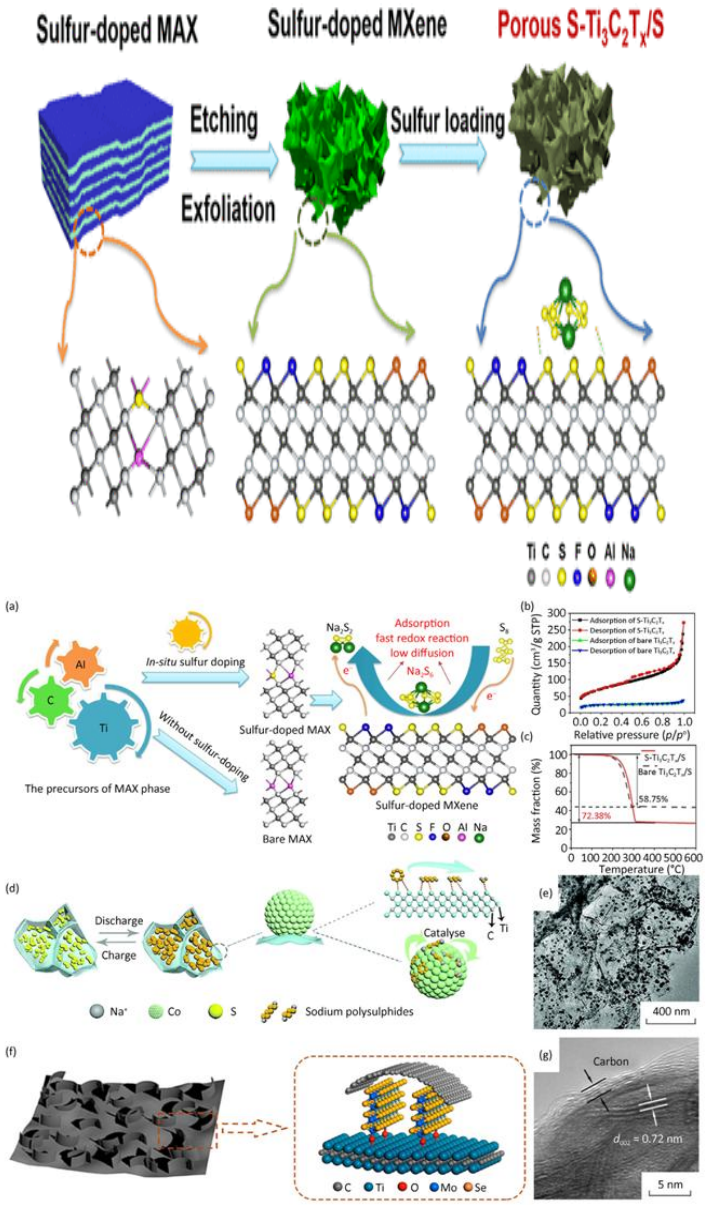

Fig 8. Situ sulfur doping strategy to prepare S-doped MXene nanosheets, a) A Schematic representation of Sulfur doping in MXene layer and chemical adsorption of sodium polysulphides on MXene b) Nitrogen adsorption-desorption curve representing the specific area of S-$Ti_3C_2T_X$ and bare $Ti_3C_2T_X$ c) TGA curve of S-$Ti_3C_2T_X$/S loaded with Sulfur. Reproduced with permission [59] copyright 2019, American Chemical Society d) Schematic catalytic effect of Co nanoparticle e) Cobalt nanoparticle with MXene represented by TEM. Reproduced with permission copyright 2020, Royal Society of chemistry f) Schematic representation of carbon-coated $MoSe_2$/MXene nanosheets g) HRTEM schematic illustration of carbon-coated $MoSe_2$/MXene material. Reproduced with permission. Copyright 2019, American Chemical Society.

Sulfur-doped MXene nanosheets (S-$Ti_3C_2T_X$) prepared by MAX precursor by doping S-heteroatom. S-$Ti_3C_2T_X$ was used as an electrode in sodium sulfur batteries with 4.5 mg cm^{-2} with 577 mAh g^{-1} at 2C, which is good electrochemical performance after 500 cycles [60]. Yunhai et al. prepared a two-dimensional nitrogen dieselinide doped vanadium carbide composite (V_4C_3@$NiSe_2$) by V_4AlC_3 using louis acid molten salt through etching procedure and afterward calcinated with selenium, which allow selenium to disintegrate into the procedure and enhance the energy density which enable $[AlCl_4]^-$ ions intercalation between layers which decrease the material loss during charging and discharging. Due to the surface modification of selenium, V_4C_3@$NiSe_2$ resulted in maintaining the stable capacity of 95 $mAgh^{-1}$ initial capacity up to 636.8 $mAgh^{-1}$ at 1 Ag^{-1} after 2700 cycles, which resulted in exploring the research towards industrialization of excellent performance rechargeable aluminium batteries [61].

3.1 Strategies for chemical modification of MXene surfaces

MXene has become highlighted as a promising member of 2D materials because MXene possesses plenty of functional groups, a large surface area, hydrophilicity, and high electrical conductivity, showing great potential in energy storage applications, but their poor flexibility, restacking, oxidation, and poor electrochemical performance are drawbacks of MXene [62]. To overcome these challenges, researchers dedicated tremendous efforts to make functional MXene by various methods, such as heteroatom-doping, polymer hybridization, organic molecule integration, and cation intercalation [63]. Heteroatom doping improves the conductivity of MXene, while cation intercalation and organic molecule integration enhance the interlayer spacing, which improves key properties and performance of MXene. Hybridizing MXene with Polymer induce the synergistic effect; also conductivity and flexibility can be improved by introducing polymer components. Although functional MXene is a prominent 2D material that enhances the physical and chemical properties of next-generation rechargeable batteries and smart materials [64], Figure 9 discusses the various strategies of surface modification with the help of MXene.

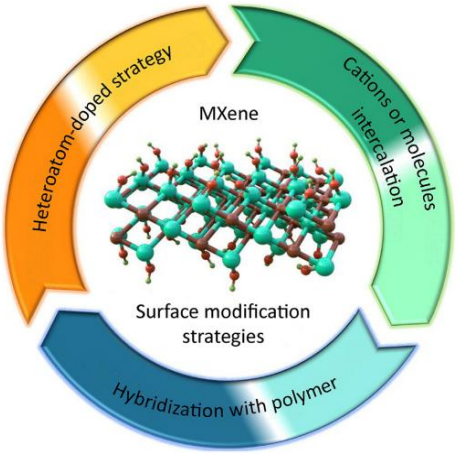

Fig.9 Strategies for MXene [65]

3.1.1 Heteroatom Doping

In MXene, heteroatom doping techniques is effective to induce a pseudocapacitance effect to enhance the intercalation and electrochemical performance. Strategies involving Nitrogen (N), Phosphorus (P), and Sulphur (S) are most commonly used due to their feasibility and efficiency to enhancing the electrochemical properties for MXene and the electrochemically active area, energy storage capacity, and catalytic performance of MXene-based materials [66]. N-doped MXene can be synthesized by using solvothermal and hydrothermal methods with uniform distribution of nitrogen atoms on MXene. Liu et al.. prepared N-doped Ti_3C_2Tx using the hydrothermal technique and use sodium dicyanamide (Nadca) as a nitrogen source and intercalant, which enhanced the interlayer spacing from 1 nm to 1.26 nm [67], as shown in Figure 10.

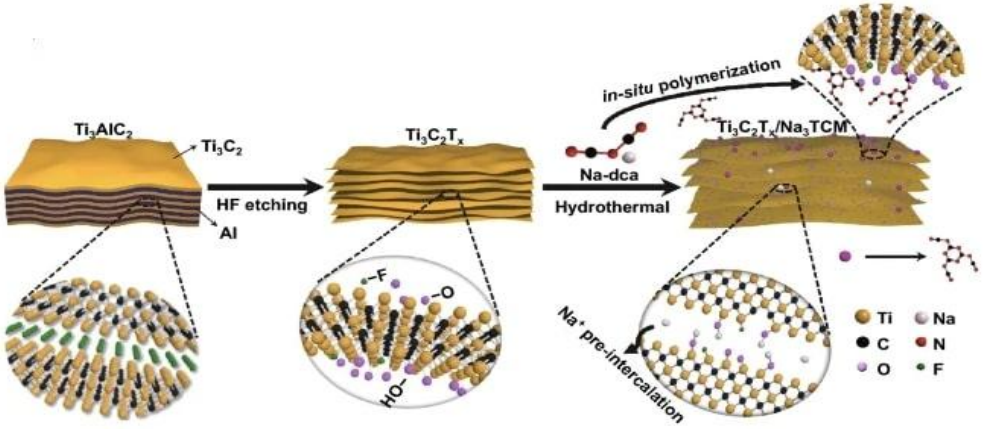

Fig.10 Schematic illustration of preparation Ti_3C_2Tx/Na_3TCM

Yang et al. [68] prepared N-dope Ti_3C_2Tx by adopting the solvothermal method using nitrogen source monoethanolamine (MEA) and urea, which resulted in fast transportation of ions and diffusion of ions due to an increase in interlayer spacing. Fan et al.. adopt an electrostatic self-assembly technique

followed by an annealing process to prepare N-doped Ti_3C_2Tx ink using melamine formaldehyde (MF) [69]. Song et al. also prepared N-doped $Ti_3C_2T_x$ using sacrificing MF as a nitrogen source at 500 ˚C by annealing technique in Ar atmosphere and used in lithium sulfur batteries (LSB) as cathode materials which resulted into restrain the shuttle effect of polysulfide with 1325 m.A.h. g^{-1} at 0.2 C storage capacity and long-term cyclic stability (0.033% degradation per cycle at 2C over 1200 cycles) [70]. Yang et al.. improved N-doped Ti_3C_2Tx, which enhances the volumetric capacitance of materials, which encourages its potential for numerous ion storage applications [71]. Sun et al.. synthesized S-doped Ti_3C_2Tx by soaking in a solution of Na_2S for 48 hours. Na+ pillar presented in between interlayer of S-doped $Ti_3C_2T_X$ which resulted to enhance the interlayer spacing from 1nm to 1.1nm and increase diffusion of ions and schematic illustration discussed in Figure.11 [71].

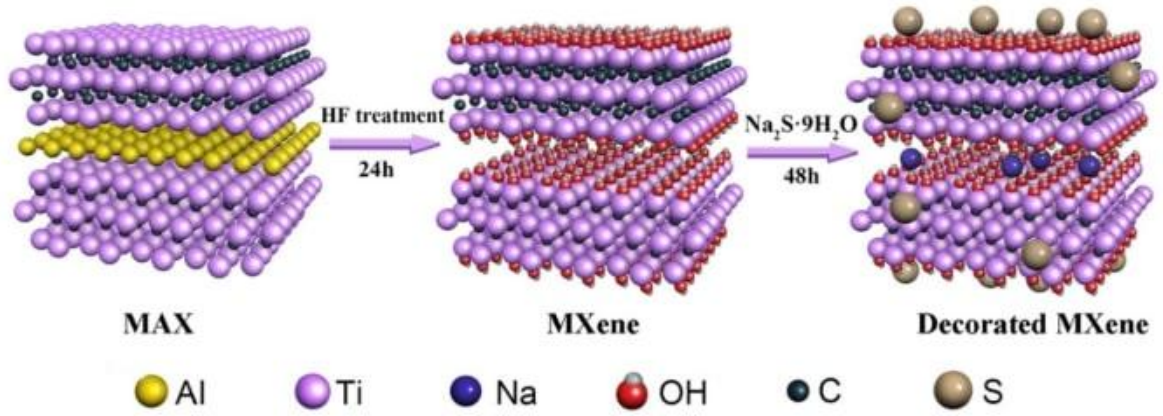

Fig. 11 Schematic illustration of S-doped MXene [72]

Zhang et al. prepared Pt doped $MO_2TiC_2O_2$-Pt_{SA} having vacancies of molybdenum, which enhance the alteration of reaction kinetics and charge transfer [73]. Wang et al used boron-carbon-nitrogen nanotubes (BCN) with cobalt doping onto TiCN to prepare a cathode TiCN-BCN-CO for zinc air batteries which provide oxygen reduction reaction (ORR) resulted into high average capacity of 701 mA.h/g with stable cycling of 200 hours [74]. Yang et al. prepared $Ti_3C_2T_X$/rGO doped with cobalt (MG-CO) nanoparticles for sulfur cathode Fig 8d-e [207, 208], which resulted in high specific capacity of 705 mA.h/g at 0.1 C with a reversible capacity of 360 mA.h/g after 200 cycles at 0.5 C [75].

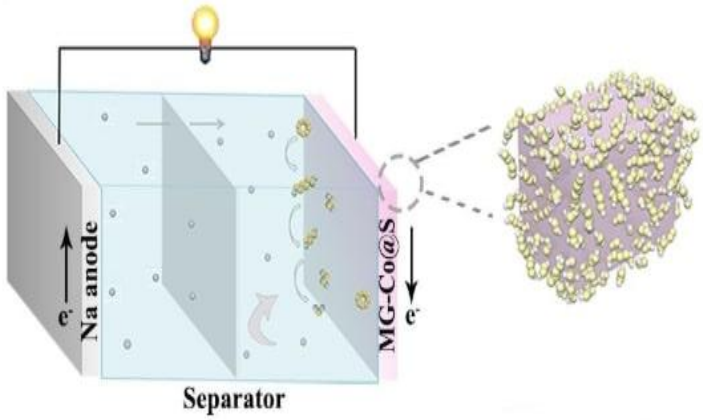

Fig.12 Schematic representation of sodium polysulfides of MG-Co@S composite during charging and discharging mechanism [76]

3.1.2 Cations or Molecule Intercalation

This method improves the capacity of energy storage with an increase in active sites, also enhancing the electrochemical performance. Lukatskaya et al. [77] increase the interlayer spacing by intercalation of numerous ions (Li+, Na+, K^+, Mg^+, NH_4^+, Al^{3+}) simultaneously on $Ti_3C_2T_x$. The interlayer spacing increases up to 0.5 ˚A when immersed in an alkali hydroxide solution, while 1˚A increase in interlayer spacing of TiC_3T_X immersed into neutral sulfate solution and remain neutral in acidic solution. Moreover, in an alkaline solution of NaOH, KOH TiC_3Tx shows a volumetric capacity of 350 F/cm^3. Li et al. [78] proposed strategies of surface modification and cation intercalation to enhance the gravimetric capacitance of $Ti_3C_2T_x$. The F-groups of $Ti_3C_2T_x$ are substituted by the -OH group after treatment with KOH at 400 ˚C, leaving Ti-active sites and removing surface terminal groups and showing gravimetric

capacitance 517 F/g at 1 mV/s (cyclic stability 99% over 10,000 cycles). Mashtalir et al.. [79] intercalated N_2H_4 on Ti_3C_2Tx into 1g/mol electrolyte of H_2SO_4, resulting in volumetric capacitance 250 F/cm^3 and gravimetric capacitance 215 F/cm^3. Luo et al. prepared Sn^{+2} and intercalated with pristine MXene to obtain a pillared Ti_3C_2 MXene matrix with cetyl-trimethylammonium bromide (CTAB), then intercalated by Sn^{+2} ion exchange with CTA^+ to modify the MXene interlayer space [209], also intercalated Sulfur on Ti_3C_2 (CT-S@Ti_3C_2) with the same idea [80]. Luo et al.. found that the interlayer space of $Ti_3C_2T_x$ with CTAB is 177% greater (2.708) than the pristine MXene with interlayer space (0.977 nm) [81]. Li et al. suggested partial sulfur doping on the surface of Ti_3C_2 MXene by HF etching Ti_3AlC_2 using thiourea as a sulfur source, which shows excellent stability as an anode in Na-ion batteries [82]. Han et al. proposed the sb/p-$Ti_3C_2T_x$ anode for sodium ion batteries by Sb ultrafine nanoparticles doping onto the few-layered MXene nanosheets (f-$Ti_3C_2T_x$), where Sb/p$Ti_3C_2T_x$ enhanced the conductivity and structural stability, and Ti-O-Sb has shown strong chemical bonding. Therefore, Na-ion batteries significantly enhanced their cyclic stability 350.6 mA.h/g with retention capacity at 50 mA.h/g after 100 cycles [83].

3.2 Impact of surface functional groups on electrochemical performance

Until now, MXene without surface termination groups has remained undiscovered. Computational research on MXene highlights the significance of surface functional groups and their impacts on stability, physiochemical characteristics, and electronic properties [84]. MXene surfaces commonly dispersed with mixed functional groups [85]. Scattering of neutrons on $Ti_3C_2T_m$ specify the van der Waals interaction between -F and -O and indicate the hydrogen bonding between -F, -O, and -OH, and stable solid electrolyte interphase (SEI) established by the -F termination while stability and thermodynamic performance of rechargeable batteries improved by -O and -OH groups [86]. Lewis etching salt method could be helpful to obtain -Cl, Br termination for future MXene application and enhance the surface modification. Therefore, meticulous surface modification of MXene-based nanocomposites is crucial for understanding their surface properties and reaction rules [87]. As MXene synthesis reaction conducted in HF solution to remove Al atomic layer which react with HF solution and various functional groups termination occur on MXene surface so they denoted as T_x. Nuclear Magnetic Resonance (NMR) spectroscopy was used to analyze surface termination of MXene [88]. Quantitative NMR suggests that -OH functional groups are less than -O, -F, while quantitative NMR confirms that there is a connection between -OH and -F. Karlsson et al [89] and Wang et al [90] demonstrated that there is no specific connection between -O and -F but they are distributed between Titanium atoms. Quantification of functional groups analysed by XPS and FTIR used to distinguish -OH, -O, -F terminations [91]. The surface termination chemical state can be identified by XAS, scanning probe microscopy, and surface morphology, while additional sensitivity of the surface is identified by ToF-SIMS. Energy dispersive x-ray spectroscopy, paired with electron microscopy, was used for surface quantification, while thermally liable quantification was analysed by TGA. As a result, functional groups have a great impact on MXene surface electronic properties, electrochemical properties, and mechanical properties [92].

3.2 Surface Coating and Thinfilm on MXene

MXene's inherent high electrical conductivity, coupled with 2D materials when delaminated into single flakes, renders them highly promising for thin-film applications. Dillon et al [93] prepared Ti_3C_2 spin cast thin films with a thickness less than 100nm, which shown bulk conductivity of 6500 S/cm. Sarycheva et el. [94] have shown bulk conductivity of 10000 S/cm with sprayed micron-thick films. MXene have the capability of conversion into aqueous solution due to their termination groups (-O, -OH, -F) which allow the fabrication of thin-film by dip coating, spray coating, and spin coating and micrometre-thick film by vacuum filtration [95].

3.3 Deposition techniques for conformal surface coatings

Deposition of solid-state MXene films ranging from nanometre to micrometre with MXene colloidal dispersion necessary for practical applications. Coating techniques refer to attaching MXenes to different substrates, which have numerous functional properties. The electrostatic interaction of MXene ensures the conformal coating on a flexible substrate and the deformability of MXene. Various printing and coating techniques have been reported to achieve MXene thin films. In Printing techniques, 3D printing and ink jet printing are known as digital printing techniques, while transfer printing and screen printing are non-digital printing techniques. MXene patterns can be obtained out of its dispersion with various coating techniques such as spray coating [96], dip coating [97], spin coating [98], Meyer-rod coating, vacuum filtration, and laser printing, which have different properties of scalability and

resolution. Each method has its limitation when fabricated ultrathin films with a thickness of 10nm on anticipated substrate. The spin coating method up to thousands of rpm formed a uniform thickness, high transmittance ultrathin MXene suitable for flexible energy storage devices [99]. The blade coating method is used in the preparation of MXene thin films by adjusting the blade height to obtain submicrometric to tens of micrometre thickness with strong toughness thin films, which can be utilized at large-scale fabrication [100]. As spray coating produces films with various surface morphologies, it has poor flake interconnectivity and low conductivity. While spin coating produces excellent flake interconnectivity and high conductivity in a film with a thickness under 10nm, which requires high concentration of MXene (over 2mg/mL), it should be performed on flat surface [101]. Kim et al.. fabricated highly conductive Ti_3C_2 MXene thin films with thickness under 10nm, including but not limited to conformal thickness of films on cylindrical substrate [102].

3.4 Role of surface coatings in enhancing stability and charge transport

Surface coating can increase the stability, electronic, chemical structural properties, and ion conductivity of MXene-based electrodes. Coating of MXene with the hydrothermal technique may not be a suitable choice because MXene is disposed to structural degradation and oxidation. But hydrothermal treatment prepares TiO2 and free carbon on MXene nanosheets; therefore a low-temperature atomic layer deposition technique is used to deposit oxides on MXene [103]. Bilal et al. perform MXene surface coating with atomic layer deposition techniques with SnO_2 and HfO_2 on copper foil up to a thickness of 100 µm with doctor blade coating that completely covered the MXene surface. SnO_2/MXene anode coated with HfO_2 shows stable specific capacity of 843 mAh/g as shown in Figure. 13 [104].

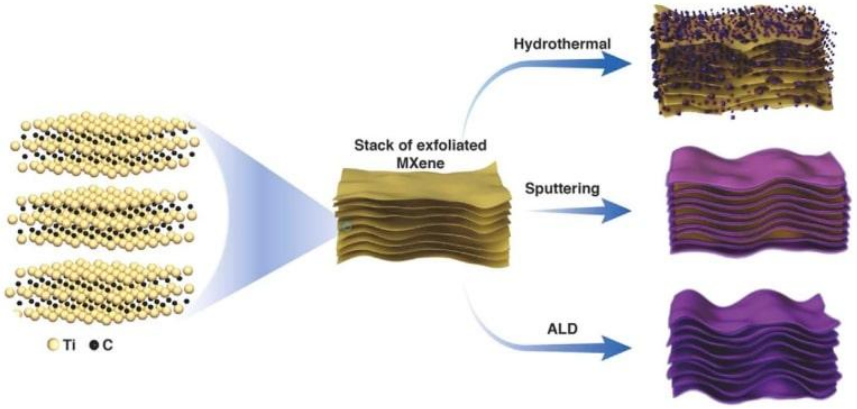

Fig. 13 Schematic illustration of SnO_2 deposition on Ti_3C_2 MXene sheets by various strategies [105]

Carbonaceous materials are applied for the surface coating of MXene due to their low cost, accessibility, high conductivity, and electrochemical stability. Huang et al. prepared $MoSe_2$/MXene@C anode for potassium ion (K-ion) batteries, which provide high capacity retention mA.h/g after 100 cycles at 200 mA/g. Carbon coating maintained the surface morphology of the MXene-based anode, which improved the rate capability, cyclic capability, and specific high capacity [106]. Yao et al.. studied that coating of ZrO_2 on $LiCoO_2$ could enhance the retention capacity to 82.5% after 100 cycles [107]. Zhang et al.. demonstrated one pot etching strategy coated fluorine-free $Ti_3C_2T_X$ cathode using hierarchical porous N-doped carbon (HPNC) which confine solubility of polysulfide, redox reaction and improve the binding energy and reduce shuttle effect. This new design of surface coating engineering improved the electrochemical performance of MXene at room temperature based on the S/Se cathode [108]. Hao wang et al synthesized 3D SCNT@MXene cages to overcome the satisfactory performance of LIS battery and its slow reaction kinetics and poor utilization of lithium cathode at high current densities. The porous 3D SCNT@MXene cages enhance the electron transportation, sulfur conductivity, and insoluble Li_2S, accommodation sulfur swelling, and electrolyte infiltration. Moreover, it improves the lithium-ion diffusion and restacking of MXene. SCNT@MXene cathode shows an initial capacity 1365.1 mA.h/g at 0.1 C and high performance (910.3 mAh/g at 1.0 C, 557.3 mAh/g at 8.0 C respectively). However, at a large current density of 6.0 C, the electrode transports 0.057% capacity decay per cycle over 700 cycles. SCNT@MXene cathode cage increases the electrochemical performance of Li- S batteries at high current density. Mallick et al. reported that in zinc ion batteries (ZIBs), cathode dissolution is a major problem. To overcome this issue, a surface coating strategy was adopted to prevent cathode dissolution in aqueous rechargeable batteries. The cyclic stability of manganese-based cathode material (MnO_2) coated with conducting polymer, carbon, and scroll graphene not only prevents cathode dissolution but also enhances the charge storage performance. α-MnO_2 coated with scroll graphene has

shown a capacity of 94% at 3 Ag^{-1} after 3000 cycles, while ZIBs have good stability without capacity decay at 0.4 Ag^{-1} of 2000 cycles [108]. Kundu et al. reported for the first time the water pillared vanadium pentoxide, Zn^{+2} ($Zn_{0.25}V_2O_5.nH_2O$) as cathode for zinc ion batteries and achieve 80% retention capacity after 1000 cycle for specific capacity of 300$mAhg^{-1}$ [219]. Coating V_2O_5 with Poly (3,4-ethlylene dioxythiophene), also known as PEDOT, resulted in achieving 232 $mAhg^{-1}$ at 20 Ag^{-1} high capability rate, and due to synergistic of PEDOT, V_2O_5 nanosheet achieve excellent cyclic stability after 1000 cycle with 89% retention at 5 Ag^{-1} [109]. Li et al coated zinc (Zn) anode with copper modified $Ti_3C_2Cl_2$ (Cu-MXene) utilizing the properties of hydrophobic and zincophilic which resulted into enhance the energy storage based on metal anodes, moreover it shows high improve cyclic stability over 1000 hours and excellent coulombic efficiency for 1100 cycles over 99.6% signifying the high stability of Zn stripping [110]. Zhang et al developed Ti_3CNT_X (MX-N) and Si/$Ti_3C_2T_X$ (MX-C) to fabricate Li-ion batteries electrodes using graphene raped silicon (Gr-Si) and nanoscale silicon powders (nSi) mixed with dispersed MXene to form a non-viscous slurry and coated on Cu foil without carbon black Figure.14-a. Graphene raped silicon coated electrode have thickness of 2100µm and nanoscale silicon powders coated electrode have thickness of 650µm indicating massive loading, and process of evaporation shown in Figure 14-b. These nanosheets enhance the electrical and mechanical properties of MXene. The performance of batteries can be improved by adding 30% of MXene into silicon powder to increase the electrical conductivity of nSi/MX-N (336 S m^{-1}), nSi/MX-C (3448 S m^{-1}), and Gr-Si/MX-C (5333 S m^{-1}), respectively. Furthermore, composite electrodes can maintain excellent mechanical flexibility and electrical conductivity in flexible and wearable electronics. In Figure.14-C, anode of nSi/MX-C represent high stability up to 280 cycle charge/discharge and shows high columbic efficiency. In Figure.14-D Gr-Si/MX-C, nSi/MX-C electrode delivered of 815 $mAhg^{-1,}$ 790 mA h g-1 with the mass loading 13 mg cm^{-2} respectively [111].

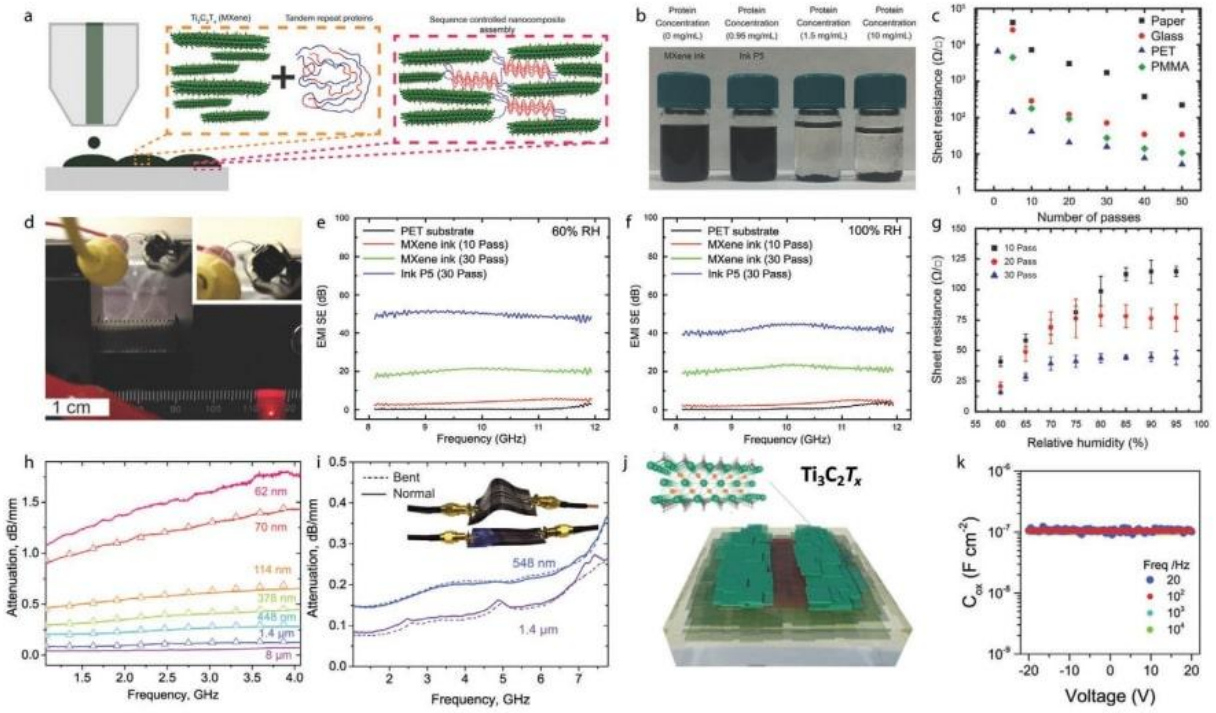

Fig.14-D Gr-Si/MX-C, nSi/MX-C electrode delivered of 815 $mAhg^{-1,}$ 790 mA h g-1

4. Surface Doping and Heteroatom Incorporation in MXenes

Pristine MXenes have large resistance, inevitable restacking, poor stability in atmospheric oxygen, and low flexibility. To overcome these drawbacks of pristine MXenes, it is crucial to use elemental doping strategies to optimize the electronic, optical, and magnetic properties. Generally, heteroatom content termed as substituted ones doped at very low levels (<=1%) and known as hetero-doped MXenes due to incorporation of heteroatoms [112].

4.1 Methods for introducing dopants and heteroatoms into MXene structures

Heteroatoms MXenes can be classified into two categories, namely in-situ and ex-situ strategies, depend upon characteristics of dopant where presynthesis of doped MAX phase require in situ strategy while postmodification of as-synthesized MXene require in ex-situ strategy [84]. Notably, doping strategies efficient increase the performance of numerous rechargeable batteries including Zn-ion, K-ion, Na-ion, Li-ion, Na-S, Li-S, Zn-air batteries [113]. Nitrogen doping can be done in both in-situ and ex-situ strategy but it is very hard to fabricate nitride MXene via wet-etching technique due to high production of energy and less stability of M-N bond. In 2012 Naguib firstly reported the fabrication of nitride doping using Ti_3AlCN by heating at 1500˚C for 2 hours and obtained an $M_3C_{2-X}AlN_x$ by varying the ratio of N/C in MAX phase. Yang et al. utilized vacuum atmospheric sintering technique to prepare $Ti_3AlC_{1.8}N_{0.2}$ with the mixture of Ti, Al, TiN, TiC with ratio 1.0:1.2:0.2:1.8. Tang et al. prepared $Ti_3AlC_{1.6}N_{0.4}$ with vacuum sintering strategy. $M_3C_{2-X}N_X$ can be prepared by a simple wet etching strategy by varying N/C ratio. Deng et al. studied that MXene-based inks can be obtained by introducing cation-induced gelatine [114]. Yu et al. developed composite inks of N-doped crumpled MXene for printable electrochemical energy storage. Controlled thickness binding-free and highly viscous inks can be obtained by mixing graphene oxide (GO) and activated carbon and carbon nanotubes (CNTs) with N-doped MXene [115]. Heteroatom doping is a powerful technique to tune the surface chemistry and bandgap of MXene. Mo doped MO_2TiC_2Tx delivered a higher capacity of 269 mAh/g than single metal TiC_2Tx, TiC_3T_x at 0.1 C. Nitrogen dope MXene NbC_2T_x has excellent cyclic stability and a high capacity of 360 mAh/g [115]. Multilayer V_2C MXene doped with Co^{+2} ions and delivered a high capacity of 1173 mAh/g at 0.1 Ag^{-1}. There are various strategies of heteroatom doping, however, to improve the performance of MXene next-generation batteries, it is highly required to adopt new and controllable strategies [116].

Intercalation agent types	Materials	Intercalation agent precursors	Methods (Temperature/C)	Interlayer spacing (nm)	added value (Δd)	Ref
				After intercalation		
Heteroatoms (N,S)	N-$Ti_3C_2T_x$	NH3	Precursor intercalation and annealing (200C)	1.23	0.27	117
	CT-S@Ti_3C_2	S	Precursor intercalation and annealing (450C)	1.37	0.39	118
Alkali metal ions	Multilayer Ti_3C_2	LiOH,NaOH, KOH,$MgSO_4$	Liquid phase intercalation (RT)	1.25	0.23	119
Metal ions (Sn4+, Co2+, Sn2+)	PVP-Sn(IV)@Ti_3C_2	$SnCl_4$	Liquid phase pre-pillaring and pillaring (RT)	1.28	0.3	119
	V_2C@Co	$Co(CH_3COO)_2$	Liquid phase pre-pillaring and pillaring (RT)	0.95	0.21	118
	CT-Sn(II)@Ti_3C_2	$SnCl_2$	Liquid phase pre-pillaring and pillaring (40 °C)	1.9	0.92	120
1D/2D nanomaterials	$Ti_3C_2T_x$/MWCNT	MWCNT	Lay-by-layer assembly (RT)	1.42	0.21	121
	MXene-rGO	rGO	Electrostatic self-assembly (RT)	1.67	0.36	122
	MoS_2-in-Ti_3C_2	MoS_2	Precursor mixing and annealing (500°C)	1.22	0.26	120

Table.2 The comparison of various MXene with interlaying spacing [120]

4.1.1 Effects of surface doping on electrochemical properties and reaction kinetics

Chemical surface doping enhances the electrochemical stability and performance of MXene. The interlayer gap in MXene can be changed by adding various intercalants. The electric double layer formed on MXene/electrolyte due to the large surface area of -OH function groups and -F terminations, which not allow desorption and adsorption of ions (e.g Na^+, Li^+, K^+) resulted in enhancing the

pseudocapacitance from Fredric redox reaction [121]. MXene doped with transition metals Ti, V, Mo undergoes a reversible redox reaction, leading to improved charge storage capacity [122]. MXene displays high electrical conductivity, which improves the transfer rate of electrons in batteries, while ion intercalation enhances the storage capacity and cyclic stability. Modification in MXene, such as hybridization, functionalization, and composite formation, increases electrochemical performance. Hybrid composite doped with MXene to improve the charge storage capacity and rate capability. Surface functionalization changes the wettability and electrical properties of MXene [123]. Heteroatom doping resolves the stacking issues in MXene. One crucial role of MXene is to enhance oxygen reduction and evolution reactions in metal-air batteries and fuel cells, leading to improved energy conversion efficiency. MXene-based batteries have the potential to develop next-generation energy storage with a longer life cycle and higher stability [124]. Doping heteroatoms N, S and metallic atoms into conductive hosts significantly improves the electrical conductivity and catalytic effect of MXene and supports chemical adsorption of the LiPSs. Zn doped MXene/S electrode with 89 wt% shows the capacity of 706 mAgh-1 at 1 C after 400 cycles much superior to S@MXene. The electrochemical performance to Li-S batteries can be enhanced by N, S doping. N-doped MXene/S electrode with 64 wt% delivers a capacity of 1072 $mAgh^{-1}$ at 0.5C and a capability rate [125].

5. Surface Roughening and Nanostructuring of MXenes

MXene possesses unique characteristics of graphene and graphene oxide, and also MXene has mechanical flexibility and lithium transport, due to which MXene is considered ideal 2D material for energy storage. The hybridization of MXene nanosheets with transition metal oxide (TMO) is well-defined and designed to discuss the unique properties. Nanostructured MXene behaves as an underlying substrate, facilitates the reverse transportation of electrons and ions at the interface, and preserves the area on MXene nanosheets. Moreover, they improve the electrochemical properties, extra active sites, and short diffusion of lithium. The porous structure of MXene has significance in improving ion diffusion in electrodes. There are various strategies to develop nanostructure MXene-based electrodes.

5.1 Techniques for Creating Hierarchical Surface Morphologies

Like 2D Material, in an electrochemical reaction, MXene nanosheets agglomerated and restacked through hydrogen bonding and vander Waals interaction. Agglomerated MXene nanosheets restrict the electrode-electrolyte-gas-triple-phase interface, limiting accessibility and ion exchange. This restriction impedes the advancement and utilization of MXene-based materials in electrolysis [126]. Moreover, the addition of an intercalant in the development of MXene hierarchical structure through assembling nanosheets, including 3-D microporous structure, MXene aerogel [127], crumbled nanosheets, and 3-D fluffy architectures, fulfills the requirements to solve the abovementioned issues. Gogotsi et al. designed Ti_3C_2 MXene with a wall thickness diameter of 1-2 μm, which reduces the ion transport lengths [128]. Wang et al designed Ti_3C_2 crumbled N-doped MXene (N-Ti_3C_2) using facile one step strategy via thermal annealing of positive charged melamine and negatively charged Ti_3C_2 MXene. The crumbled N-Ti_3C_2 have ideal polysulfide adsorption characteristics, high surface area, and high reversible capacity of 1144 mAh/g at 0.2 C (1 C = 1673 mA/g), 770 mAh/g at 2 C [118]. Yang et al. adopted a technique of facile self-assembly to design 3-D MXene hydrogel in the presence of Ethylenediamine (EDA) and graphene oxide (GO) [119]. The obtained gelatine has a high surface area, 3-D conductive framework, high robustness, and good process ability, which proved as a flexible host with hierarchical hybrid nanostructure for energy storage and conversion [129].

This shortcoming causes to degrades the performance of MXene-based electrodes in batteries due to decreased surface area and electronic and ionic transportation towards electrodes. Recently, several studies have focused on a combination of TMO (Fe_2O_3, MnO_2) on the outer surface of stacked MXene thick-films, leaving a substantial fraction of MXene surface area unutilized [130]. MXene contains functional groups such as -O, -OH, and -F, which provide good solubility to dissolve in solvents like N, Ndimethylformaldehyde, dimethyl sulfoxide, acetone, ethanol, and water. Liu et al reported Vander Waal interaction route to assemble the TMO on surface of MXene (Ti_3C_2) which was first study to decorate TMO including SnO_2 nanowires and TiO_2 nanorods on individual MXene surface where MXene nanosheets facilitate the reverse transportation of ions and electrons and prevent the TMO nanostructure from coalescing during the lithiation and delithiation. In the Vander Waal interaction route, MXene mixed with nanostructures of TMO and tetrahydrofuran (THF), which resulted in assembled TMO nanostructures forming micelle-like heterostructure on the surface of MXene.

However, results revealed that SnO_2/MXene and TiO_2/MXene heterostructure exhibited high rate performance without electrolytic optimization and surface encapsulation and may be ideal candidates for next generation high-energy and high-power lithium-ion batteries [131]. TiO_2 nanorods and SnO_2 nanowires assembling over MXene nanosheets are represented in Figure. 15

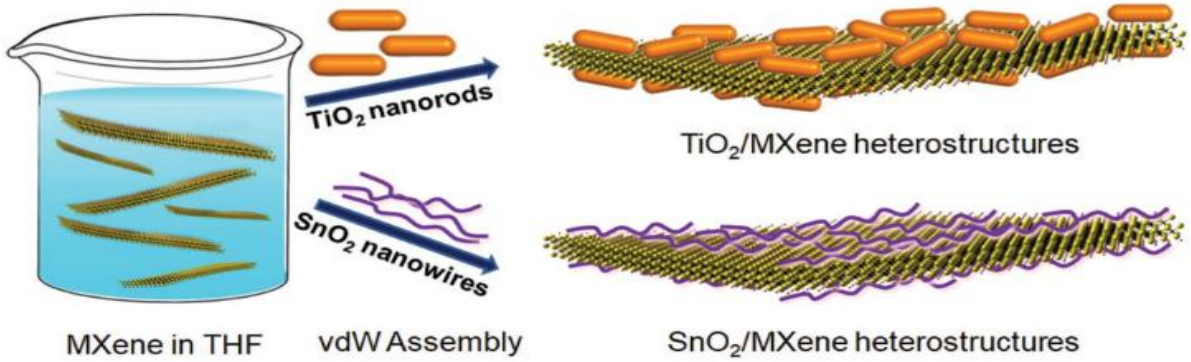

Figure.15 Schematic diagram of assembling TiO_2 nanorods and SnO_2 nanowires MXene nanosheets in THF via Vander Waals Interaction [132].

5.2 Impact of nanostructured surfaces on energy storage performance

Recent studies provide overview on MXene nanostructure (MXene/0-D, MXene/1-D, MXene/2-D) for diversified metal ion batteries (MIBs) from lithium ion batteries (LIBs), sulfur ion batteries (SIBs) to various new type of batteries such as potassium ion batteries (PIBs), magnesium ion batteries (MgIBs), zinc ion batteries (ZnIBs), calcium ion batteries (CIBs) which consist of loaded, encapsulated, sandwiched model are first classified models for MXenes highlighted the advance hybrid electrodes which improve the structure stability, optimize the transfer of ions/electrons and resolve the major challenges in advancement of MIBs. The electrochemical performance of MXene depends upon the micro and nanostructure of MXene (interlayer, spacing, pores), functional groups (-O, -OH, -F), and chemical components (type of M, X, and dopant material). The common vapor deposition method (CVD) proved to be an excellent strategy to fabricate high-quality of MXene nanostructured films [133]. MXene has been utilized to develop advanced nanostructure for electrochemical energy storage and improve the performance of lithium sulfur batteries, electrolysis, and (Li^+, Na^+, K^+) metal ion batteries (MIBs) [134]. The Typical nanostructure with 1-D, such as nanotubes, nanowires, nanobelts, and nanorods attracted attention due to their properties and potential application in scientific research [135]. Xiao et al.. used a hydrothermal and electrostatically driven method to design $Ti_3C_2T_x$/Cds by growing Cds nanorods on the surface of ultrathin $Ti_3C_2T_X$ nanosheets, and EDS results revealed good integration and short heterostructure confinement of 2D $Ti_3C_2T_x$/Cds than 1-D Cds [136]. Lin et al.. used radio frequency plasma molecular beam epitaxy (MBE) to develop 1D MXene/InGaN nanorod heterostructure on Si substrate and MXene Ti_3C_2Tx films [137]. Moreover, Gogotsi et al.. developed a sandwich-like heterostructure of $Ti_3C_2T_X$/CNT by alternating filtration of CNT, which possess ordered structure [138]. These heterostructures have the advantage of 1-D nanostructures and 2-D MXene to improve the performance of MXene in energy storage applications due to the synergistic effect [139]. Cui et al. designed 2-D MXene nanosheet heterostructure of Nb_2CT_x/Bi_2WO_6 by adopting the facile hydrothermal technique. A variety of hierarchical nanostructure 2-D MXene have been developed to enhance the performance and satisfy the requirements of batteries and energy storage applications [113]. Yu et al. designed 2-D MXene $Ti_3C_2T_X$/rGO composite aerogel with a 3-D hierarchical nanostructure by adopting an ice template strategy. $Ti_3C_2T_X$/rGO have a large surface area of MXene and rGO, high conductivity of MXene which prevent poor restacking of MXene and also resist poor oxidization of MXene [140].

Wang et al. reported green and facile synthesis of S-CNT_S MXene to assemble micro-cages which can be used in Li-S batteries as cathode material, and resulted into enhance the current density, cyclic stability and improve the storage capacity. S-CNTs were prepared with sulfur diameter 5-8nm in situ synthesized on the CNT_S surface, then MXene nanosheets of ultrathin Ti_3C_2Tx wraped around S-CNTS to form 3D S-CNT_S hollow microsphere cages and behave as cathode material in Batteries. S-CNT_S microsphere hollow cages improve electron/ion transfer, enhance the reaction kinetics, avoid the shuttle effect of lithium polysulfides (LiPSs), and control empty spaces within the microsphere cages. S-CNT_S delivered excellent current density (557.3, 910.3 $mAhg^{-1}$ at 8.0 and 1.0 C respectively), high specific

capacity of 1375.1 mAh^{-1} at 1.0 C. Significantly, electrodes attained high capacity of 645.5 $mAhg^{-1}$ at 4.0 C after 150 cycles at a retention of 656.3 $mAhg^{-1}$. Furthermore, over 700 cycles at a large current density electrode decay 0.057% capacity decay per cycle. LiS batteries microsphere cathode cages can enhance the electrochemical storage performance at high current densities and at fast charge discharge energy storage systems [141].

6. Surface Passivation and Interface Engineering in MXene Electrodes

MXene electrodes attracted considerable attention as electrode materials to improve the electrochemical performance of batteries, long-time operation stability, high power, fast charging capabilities, and high energy densities. There are a variety of MXene compositions that show unique capabilities and characteristics for energy storage [142]. MXene electrode formation occurs via fradric and non-fradric processes when interacting with the electrolyte solution. Moreover, in MXene, the charge storage mechanism depends upon the surface chemistry and their morphology [142]. Das et al. demonstrated that surface engineering plays a significant role in enhancing charge storage capacities and improving functional properties of MXene [143].

6.1 Strategies for stabilizing MXene surfaces and electrode-electrolyte interfaces

Chemical modification is a promising strategy to improve the stability of MXene and control the surface properties of materials. Jingjing et al. modified $Ti_3C_2T_X$ by co-polycondensation of hydroxyl groups and hydrolysis of silane and obtained 3-Aminopropy triethoxysilane functioned MXene (APTES-MXene). Obtained APTES-MXene transform nanosheets of MXene into thermodynamically stable metal oxides, which demonstrated functional MXene have grafted coatings with surface characteristics from hydrophobic and hydrophilic, also enhanced stability of MXene [144]. Kim et al. demonstrated stable dispersion of $Ti_3C_2T_X$ using deep eutectic solvent (DEESs) and dispersion strategy, which prevent MXene nanosheets from oxidation in aqueous and dried state. Fabrication of MXene with assisted MXene is simple and low cost. Moreover, DEEs enhance the electrochemical stability of MXene nanosheets due to hydrogen and surface passivation [145]. Zhao et al.. used a facile strategy to improve the surface stability of MXene ($Ti_3C_2T_X$) by chemical modification of copper (Cu) foam on $Ti_3C_2T_X$ nanosheets and obtained a 3d collector (MXene@CF) fabricated on a dendrite-free lithium anode. MXene@Cf demonstrated better cyclic stability than bare Cu-foam-based fuel cells, and this strategy improved the lithium deposition. Moreover, termination groups of fluorine in MXene contributed to forming the stable solid electrolyte interphase (SEI); therefore, MXene@CF preserved the 98% columbic efficiency 1 mA cm^{-2} after 200 cycles and worked up to 1000 hours without any fluctuation in intense voltage [146].

Sun et al. developed low-cost, dendrite-free metal batteries by studying the mechanism of MXene ($Ti_3C_2T_X$) in an aqueous electrolyte on a zinc (Zn) electrode with the formation of MXene film on the surface of Zn foil. MXene film becomes denser and denser with adding more concentration of MXene. After soaking for 4 hours, electrolytes of MXene-ZSO 0.02, MXene-ZSO 0.05, and MXene-ZSO 0.1 show the thickness of 0.3, 0.5, and 1.0 µm. Results revealed that MXene absorbed on Zn foil in ZSO electrolyte demonstrated the columbic efficiency of 99.7% and excellent reversibility up to 1180 cycles at 2 mA cm^{-2}. However, the fabrication of MXene-added Zn-V_2O_5 electrolytes revealed the cyclic stability up to 300 cycles, high specific capacity 326.4 $mAhg^{-1}$ at 1 $Ag^{-1,}$ and high rater capability of 190.5 $mAhg^{-1}$ at 4 Ag^{-1} [147] [148]. Qiao et al. designed a Zn//KMO/Ti_3C_2 battery by employing an MXene skeleton ($Ti_3C_2T_X$) attached with electrolyte K_2SO_4 to improve the cathode δ-MnO_2 structure stability. δ-MnO_2/Ti_3C_2Tx cathode promoting the Mn^{+2} electrodeposition and show specific synergistic effect with K_2SO_4 electrolyte. However, the stripping/plating of Zn anode reversibility can be enhanced by manipulating the development of zinc dendrites. Consequently, specific capacity of Zn//KMO/Ti_3C_2 battery reaches upto 502.2 $mAgh^{-1}$ and 371.1 $mAgh^{-1}$ at 0.3 $mAgh^{-1}$, 2 Agh^{-1} respectively. Furthermore, it shows 93.3% capacity retention at a current density of 10 Ag^{-1} after 9500 cycles. Moreover, the dendrite-free Zn anode delivered columbic efficiency of 99.9% after 2300 cycles [148]. Hsiao et al. reported the synthesized $Ti_4N_3T_X$ MXene and discussed the characteristics of multi-layered $Ti_4N_3T_X$ MXene in electrochemical activation of electrolytes with continuous cation intercalation to access redox active sites at 50 mVS^{-1} cyclic voltammetry performance over 10 10-day period. Consequently, resulted in enhanced capacitance of 140% in $MgSO_4$, 300% in H_2SO_4, and 500% in KOH at 2 mVS^{-1} maintaining after 5000 cycles as well as proved as stable MXene to store electrochemical energy [149].

6.2 Role of interfacial engineering in improving cycling stability and efficiency

Bilal et al. reported that the performance of SnO_2/MXene-based anode improved by introducing a thin passivation layer of HfO_2 by ALD reactor which behave as solid electrolyte interphase (SEI) in batteries. This proposed design improved the MXene-based anode cyclic stability and high-capacity performance [150]. Zou et al. designed a nanocomposite of sandwiched structured Co-NiS/MXene and various MXene composites, which shows the maximum electrochemical performance of sodium-ion batteries and lithium-ion batteries. For LIBs, it can deliver a high capacity of 911 $mAhg^{-1}$ as well as a specific high capacity of 1119 $mAgh^{-1}$ at 0.1 Ag^{-1} and 509 $mAgh^{-1}$ at 2 Ag^{-1} after 200 cycles. Moreover, for sodium-ion batteries, Co-NiS/MXene delivers a maximum rate capability of 263 $mAhg^{-1}$ at 5 Ag^{-1} and a maximum discharge capacity rate of 541 $mAhg^{-1}$ at 0.1 Ag^{-1}. This interfacial self-assembly technique is highly recommended to researchers to fabricate other sandwiched structure MXene-based nanocomposite [151]. Sha et al. developed VSe_2@V_2CTx by the surface salinization method due to which MXene supplied a source of metal for TMSe. VSe_2@V_2CTx preserves the structure of nanoplates from restacking and shows superb efficiency for aqueous zinc ion batteries with a capacity of 158.1 $mAhg^{-1}$ after 600 cycles at 2 Ag^{-1} [152]. Li et al. suggested heteroatomic interface engineering of octahedron composite of VSe_2-ZrO_2/C/MXene through a hybrid two step method of metal-organic frameworks resulted to enhance the electrochemical stability and performance of lithium ion batteries. Subsequently, VSe_2-ZrO_2/C/MXene show a long-term capacity of 430 $mAhg^{-1}$ at 1.0 Ag^{-1} after 1000 cycles and a high reversible capacity of 1238.5 $mAgh^{-1}$ at 100 $mAg^{-1,}$ which proved as a new attempt based on MOF/MXene-derived selenide electrode for energy storage applications [153]. Wang et al represent MXene as excellent electrode material for sodium ion batteries (SIBs), due to negative charge on functional groups and sluggish ion-diffusion reaction kinetics. Herein Wang et al proposed positively charged conductive polyaniline (PANI) to develop a 3-D network of PANI/$Ti_3C_2T_X$ to enhance the electronic and ionic conductivities. The combination of 3D network and surface engineering of PANI/$Ti_3C_2T_X$ shows superb sodium storage performance with efficient capacity, ultralong lifespan at high current density, and efficient electrochemical performance at temperature +50 to -30 ˚C [154].

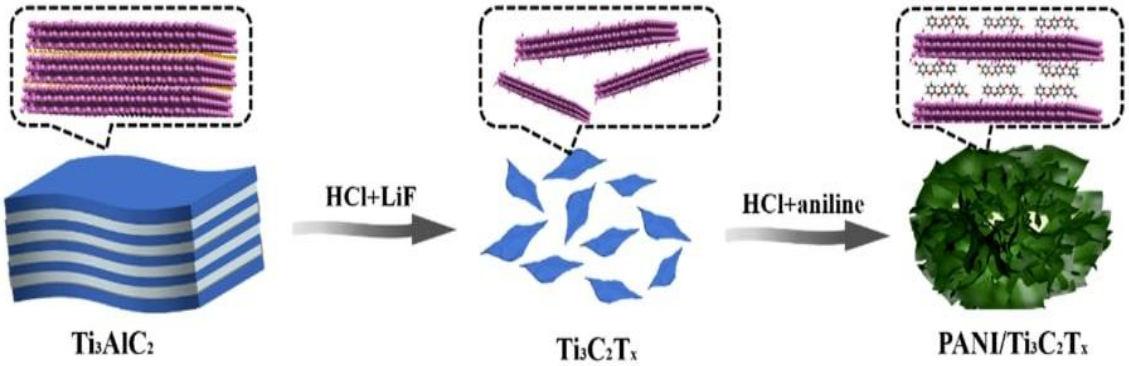

Fig. 16 Schematic illustration of synthesis via self-assembly [155]

7. Conclusions and Future Outlook

Recent advances in MXene and MXene-based electrodes have shown remarkable achievements and performance in electrochemical energy storage in academic research and industrial applications. Still there are many challenges that are involved in developing massive production of MXene-based electrodes with excellent properties in next-generation rechargeable batteries.

7.1 Summary of key advances in surface engineering of MXenes

Surface engineering strategies enhance the electrochemical performance of MXene-based electrodes by adjusting the various aspects, including chemical composition, surface terminations, and interlayer spacing. Introducing the various carbon-based materials, silicon, and metal-oxide not only enhances the capacity of MXene to store charge but also prevents the MXene single layer from stacking, which was a key challenge to enhance the electrochemical performance of MXene-based electrodes due to engineering and optimizing their chemical composition. The structure of MXene and advancement in MXene-hybrid materials improve the stability, electron/ion transportation, and their electronic conductivity and overcome the major challenge of high ion diffusion resistance at high current densities, which decrease the capability rate of MXene-based electrodes. MXene has helped to achieve high

capacity and fast charge-discharge by the advantage of its surface chemistry and interlayer spacing. Additionally, heteroatom doping enhances the dopants' interaction with electrolytes and improves the electronic characteristics of electrodes. As in Li-S batteries theoretical specific capacity was measured 1675 $mAhg^{-1}$ while SCNT doped MXene cathode enhance the electrochemical performance in Li-S due to insoluble nature of Li_2-S, preventing the restacking of MXene achieve the initial capacity 1365.1 $mAhg^{-1}$ at 0.1C, and achieve the high performance of 910.3 $mAhg^{-1}$ at 1.0 C, and 557.3 $mAhg^{-1}$ at 8.0 C respectively, electrode transports 0.057% over 700 cycle capacity decay per cycle due surface engineering of MXene. SCNT/MXene and Zn/KMO/Ti_3C_2 enhance the specific capacity, excellent stability, and minimum decay rates. α-MnO_2 over $Ti_4N_3T_X$ show excellent performance over thousands of cycles. This variety of surface engineering and modification of MXene makes it highly adaptable across next-generation batteries and electrochemical applications.

7.2 Remaining challenges and opportunities for further improvements

To design future MXene-based electrodes to enhance the electrochemical performance of next-generation batteries, researchers should find efficient, safe, and high-quality strategies to develop MXene-based electrodes. There are various theoretical studies on MXene-based electrodes multivalent ions (Zn^{+2}, Mg^{+2}, Ca^{+2}, Al^{+3}) batteries, which have no predicted performance as reported. Theoretically, lithium cathode air batteries should be investigated based on MXene-based electrodes. Operando characterization strategy must be used to ensure the mechanism of the above multivalent ion batteries as predicted in sodium and potassium ion batteries with MXene-based electrodes to understand the problem and possible solution. Researchers have primarily focused on the development of the electrochemical properties of active materials, and they established the MXene-based batteries using coin cells; however, in the future, it will be transformed into pouch-type assemble batteries with flexible devices. Therefore, the major focus should be on the development of solid-state electrolytes that contain the excellent properties of flexible MXene-based electrodes. MXene's as electrodes to store energy tackle various obstacles, and this tendency will continue in the future.

References

1. Pang, J., Mendes, R. G., Bachmatiuk, A., Zhao, L., Ta, H. Q., Gemming, T., ... & Rummeli, M. H. (2019). Applications of 2D MXenes in energy conversion and storage systems. Chemical Society Reviews, 48(1), 72-133.
2. Gogotsi, Y., & Anasori, B. (2019). The rise of MXenes. ACS nano, 13(8), 8491-8494.
3. Sun, W., Shah, S. A., Chen, Y., Tan, Z., Gao, H., Habib, T., ... & Green, M. J. (2017). Electrochemical etching of Ti 2 AlC to Ti 2 CT x (MXene) in low-concentration hydrochloric acid solution. Journal of Materials Chemistry A, 5(41), 21663-21668.
4. Lee, D. K., Chae, Y., Yun, H., Ahn, C. W., & Lee, J. W. (2020). CO2-Oxidized Ti3C2T x–MXenes Components for Lithium–Sulfur Batteries: Suppressing the Shuttle Phenomenon through Physical and Chemical Adsorption. ACS nano, 14(8), 9744-9754.
5. Li, X., Wang, C., Cao, Y., & Wang, G. (2018). Functional MXene materials: progress of their applications. Chemistry–An Asian Journal, 13(19), 2742-2757.
6. Li, X., Wang, C., Cao, Y., & Wang, G. (2018). Functional MXene materials: progress of their applications. Chemistry–An Asian Journal, 13(19), 2742-2757.
7. Zhang, C., Anasori, B., Seral-Ascaso, A., Park, S. H., McEvoy, N., Shmeliov, A., ... & Nicolosi, V. (2017). Transparent, flexible, and conductive 2D titanium carbide (MXene) films with high volumetric capacitance. Advanced materials, 29(36), 1702678.
8. Aslam, M. K., Niu, Y., & Xu, M. (2021). MXenes for non-lithium-ion (Na, K, Ca, Mg, and Al) batteries and supercapacitors. Advanced Energy Materials, 11(2), 2000681.
9. Bhat, A., Anwer, S., Bhat, K. S., Mohideen, M. I. H., Liao, K., & Qurashi, A. (2021). Prospects challenges and stability of 2D MXenes for clean energy conversion and storage applications. npj 2D Materials and Applications, 5(1), 61.
10. Li, J., Guo, C., & Li, C. M. (2020). Recent Advances of Two-Dimensional (2 D) MXenes and Phosphorene for High-Performance Rechargeable Batteries. ChemSusChem, 13(6), 1047-1070.
11. Ronchi, R. M., Arantes, J. T., & Santos, S. F. (2019). Synthesis, structure, properties and applications of MXenes: Current status and perspectives. Ceramics International, 45(15), 18167-18188.
12. Zhang, T., Zhang, L., & Hou, Y. (2022). MXenes: Synthesis strategies and lithium-sulfur battery applications. EScience, 2(2), 164-182.
13. Dong, Y., Shi, H., & Wu, Z. S. (2020). Recent advances and promise of MXene-based nanostructures for high-performance metal ion batteries. Advanced Functional Materials, 30(47), 2000706.
14. Gervillié-Mouravieff, C., Boussard-Plédel, C., Huang, J., Leau, C., Blanquer, L. A., Yahia, M. B., ... & Tarascon, J. M. (2022). Unlocking cell chemistry evolution with operando fibre optic infrared spectroscopy in commercial Na (Li)-ion batteries. Nature Energy, 7(12), 1157-1169.
15. Yu, Y., Zhou, J., & Sun, Z. (2019). Modulation engineering of 2D MXene-based compounds for metal-ion batteries. Nanoscale, 11(48), 23092-23104

16. Liu, B., Fang, R., Xie, D., Zhang, W., Huang, H., Xia, Y., ... & Tu, J. (2018). Revisiting scientific issues for industrial applications of lithium–sulfur batteries. Energy & Environmental Materials, 1(4), 196-208.
17. Seh, Z. W., Sun, Y., Zhang, Q., & Cui, Y. (2016). Designing high-energy lithium–sulfur batteries. Chemical society reviews, 45(20), 5605-5634.
18. Kong, L., Peng, H. J., Huang, J. Q., Zhu, W., Zhang, G., Zhang, Z. W., ... & Zhang, Q. (2017). Beaver-dam-like membrane: a robust and sulphifilic MgBO2 (OH)/CNT/PP nest separator in Li-S batteries. Energy Storage Materials, 8, 153-160.
19. Jeong, Y. C., Kim, J. H., Kwon, S. H., Oh, J. Y., Park, J., Jung, Y., ... & Park, C. R. (2017). Rational design of exfoliated 1T MoS 2@ CNT-based bifunctional separators for lithium sulfur batteries. Journal of materials chemistry A, 5(45), 23909-23918.
20. Li, N., Xie, Y., Peng, S., Xiong, X., & Han, K. (2020). Ultra-lightweight Ti3C2Tx MXene modified separator for Li–S batteries: thickness regulation enabled polysulfide inhibition and lithium ion transportation. Journal of Energy Chemistry, 42, 116-125.
21. Wang, D., Gao, Y., Liu, Y., Gogotsi, Y., Meng, X., Chen, G., & Wei, Y. (2017). Investigation of chloride ion adsorption onto Ti 2 C MXene monolayers by first-principles calculations. Journal of Materials Chemistry A, 5(47), 24720-24727.
22. Wang, D., Gao, Y., Liu, Y., Jin, D., Gogotsi, Y., Meng, X., ... & Wei, Y. (2017). First-principles calculations of Ti2N and Ti2NT2 (T= O, F, OH) monolayers as potential anode materials for lithium-ion batteries and beyond. The Journal of Physical Chemistry C, 121(24), 13025-13034.
23. Pomerantseva, E., & Gogotsi, Y. (2017). Two-dimensional heterostructures for energy storage. Nature Energy, 2(7), 1-6.
24. Aierken, Y., Sevik, C., Gülseren, O., Peeters, F. M., & Çakır, D. (2018). MXenes/graphene heterostructures for Li battery applications: a first principles study. Journal of Materials Chemistry A, 6(5), 2337-2345.
25. Tahini, H. A., Tan, X., & Smith, S. C. (2017). The origin of low workfunctions in OH terminated MXenes. Nanoscale, 9(21), 7016-7020.
26. Wang, Y., Chen, R., Chen, T., Lv, H., Zhu, G., Ma, L., ... & Liu, J. (2016). Emerging non-lithium ion batteries. Energy Storage Materials, 4, 103-129.
27. Castelvecchi, D., & Stoye, E. (2019). World-changing batteries win Nobel. Nature, 574(7778), 308.
28. Yang, C., Xin, S., Mai, L., & You, Y. (2021). Materials design for high-safety sodium-ion battery. Advanced Energy Materials, 11(2), 2000974.
29. Alhabeb, M., Maleski, K., Anasori, B., Lelyukh, P., Clark, L., Sin, S., & Gogotsi, Y. (2017). Guidelines for synthesis and processing of two-dimensional titanium carbide (Ti3C2T x MXene). Chemistry of Materials, 29(18), 7633-7644.
30. Jeon, J., Park, Y., Choi, S., Lee, J., Lim, S. S., Lee, B. H., ... & Lee, S. (2018). Epitaxial synthesis of molybdenum carbide and formation of a Mo2C/MoS2 hybrid structure via chemical conversion of molybdenum disulfide. ACS nano, 12(1), 338-346.
31. Zhang, C. J., Pinilla, S., McEvoy, N., Cullen, C. P., Anasori, B., Long, E., ... & Nicolosi, V. (2017). Oxidation stability of colloidal two-dimensional titanium carbides (MXenes). Chemistry of Materials, 29(11), 4848-4856.
32. Rozmysłowska, A., Wojciechowski, T., Ziemkowska, W., Chlubny, L., Olszyna, A., Poźniak, S., ... & Jastrzębska, A. M. (2018). Colloidal properties and stability of 2D Ti3C2 and Ti2C MXenes in water. International Journal of Electrochemical Science, 13(11), 10837-10847.
33. Chen, J., Liu, M., Huang, H., Deng, F., Mao, L., Wen, Y., ... & Wei, Y. (2018). Facile preparation of thermoresponsive fluorescent silica nanopaprticles based composites through the oxygen tolerance light-induced RAFT polymerization. Journal of Molecular Liquids, 259, 179-185.
34. Chen, J., Huang, Q., Huang, H., Mao, L., Liu, M., Zhang, X., & Wei, Y. (2020). Recent progress and advances in the environmental applications of MXene related materials. Nanoscale, 12(6), 3574-3592.
35. Qin, L., Tao, Q., Liu, X., Fahlman, M., Halim, J., Persson, P. O., ... & Zhang, F. (2019). Polymer-MXene composite films formed by MXene-facilitated electrochemical polymerization for flexible solid-state microsupercapacitors. Nano Energy, 60, 734-742.
36. Zhu, X., Liu, B., Hou, H., Huang, Z., Zeinu, K. M., Huang, L., ... & Yang, J. (2017). Alkaline intercalation of Ti3C2 MXene for simultaneous electrochemical detection of Cd (II), Pb (II), Cu (II) and Hg (II). Electrochimica Acta, 248, 46-57.
37. Tian, Y., Que, W., Luo, Y., Yang, C., Yin, X., & Kong, L. B. (2019). Surface nitrogen-modified 2D titanium carbide (MXene) with high energy density for aqueous supercapacitor applications. Journal of materials chemistry A, 7(10), 5416-5425.
38. Liu, P., Ding, W., Liu, J., Shen, L., Jiang, F., Liu, P., ... & Xu, J. (2020). Surface termination modification on high-conductivity MXene film for energy conversion. Journal of Alloys and Compounds, 829, 154634.
39. Lin, H., Wang, X., Yu, L., Chen, Y., & Shi, J. (2017). Two-dimensional ultrathin MXene ceramic nanosheets for photothermal conversion. Nano letters, 17(1), 384-391.
40. Li, Z., Zhuang, Z., Lv, F., Zhu, H., Zhou, L., Luo, M., ... & Guo, S. (2018). The marriage of the FeN4 moiety and MXene boosts oxygen reduction catalysis: Fe 3d electron delocalization matters. Advanced materials, 30(43), 1803220.
41. Xia, Y., Mathis, T. S., Zhao, M. Q., Anasori, B., Dang, A., Zhou, Z., ... & Yang, S. (2018). Thickness-independent capacitance of vertically aligned liquid-crystalline MXenes. Nature, 557(7705), 409-412.
42. Maleski, K., Mochalin, V. N., & Gogotsi, Y. (2017). Dispersions of two-dimensional titanium carbide MXene in organic solvents. Chemistry of Materials, 29(4), 1632-1640.
43. Wang, H. W., Naguib, M., Page, K., Wesolowski, D. J., & Gogotsi, Y. (2016). Resolving the structure of Ti3C2T x MXenes through multilevel structural modeling of the atomic pair distribution function. Chemistry of Materials, 28(1), 349-359.
44. Harris, K. J., Bugnet, M., Naguib, M., Barsoum, M. W., & Goward, G. R. (2015). Direct measurement of surface termination groups and their connectivity in the 2D MXene V2CT x using NMR spectroscopy. The Journal of Physical Chemistry C, 119(24), 13713-13720.

45. Hope, M. A., Forse, A. C., Griffith, K. J., Lukatskaya, M. R., Ghidiu, M., Gogotsi, Y., & Grey, C. P. (2016). NMR reveals the surface functionalisation of Ti 3 C 2 MXene. Physical Chemistry Chemical Physics, 18(7), 5099-5102.
46. Yu, T., Zhao, Z., Liu, L., Zhang, S., Xu, H., & Yang, G. (2018). TiC3 monolayer with high specific capacity for sodium-ion batteries. Journal of the American Chemical Society, 140(18), 5962-5968.
47. Wang, X., Shen, X., Gao, Y., Wang, Z., Yu, R., & Chen, L. (2015). Atomic-scale recognition of surface structure and intercalation mechanism of Ti3C2X. Journal of the American Chemical Society, 137(7), 2715-2721.
48. Naguib, M., Adams, R. A., Zhao, Y., Zemlyanov, D., Varma, A., Nanda, J., & Pol, V. G. (2017). Electrochemical performance of MXenes as K-ion battery anodes. Chemical communications, 53(51), 6883-6886.
49. Wang, J., Xie, G., Yu, C., Peng, L., Zhu, Y., Xie, X., & Zhang, N. (2022). Stabilizing Ti3C2T x in a Water Medium under Multiple Environmental Conditions by Scavenging Oxidative Free Radicals. Chemistry of Materials, 34(21), 9517-9526.
50. Xie, X., Chen, C., Zhang, N., Tang, Z. R., Jiang, J., & Xu, Y. J. (2019). Microstructure and surface control of MXene films for water purification. Nature Sustainability, 2(9), 856-862.
51. Xu, J., Liu, Z., Wang, Q., Li, J., Huang, Y., Wang, M., ... & Chen, C. (2023). Facile tailoring of surface terminations of MXenes by doping Nb element: toward extraordinary pseudocapacitance performance. ACS Applied Materials & Interfaces, 15(12), 15367-15376.
52. Li, G., Lian, S., Wang, J., Xie, G., Zhang, N., & Xie, X. (2023). Surface chemistry engineering and the applications of MXenes. Journal of Materiomics.
53. Harris, K. J., Bugnet, M., Naguib, M., Barsoum, M. W., & Goward, G. R. (2015). Direct measurement of surface termination groups and their connectivity in the 2D MXene V2CT x using NMR spectroscopy. The Journal of Physical Chemistry C, 119(24), 13713-13720.
54. Karlsson, L. H., Birch, J., Halim, J., Barsoum, M. W., & Persson, P. O. (2015). Atomically resolved structural and chemical investigation of single MXene sheets. Nano letters, 15(8), 4955-4960.
55. Wang, X., Shen, X., Gao, Y., Wang, Z., Yu, R., & Chen, L. (2015). Atomic-scale recognition of surface structure and intercalation mechanism of Ti3C2X. Journal of the American Chemical Society, 137(7), 2715-2721.
56. Mičušík, M., Šlouf, M., Stepura, A., Soyka, Y., Ovodok, E., Procházka, M., & Omastová, M. (2023). Aging of 2D MXene nanoparticles in air: an XPS and TEM study. Applied Surface Science, 610, 155351.
57. Song, Y., Sun, Z., Fan, Z., Cai, W., Shao, Y., Sheng, G., ... & Sun, J. (2020). Rational design of porous nitrogen-doped Ti3C2 MXene as a multifunctional electrocatalyst for Li–S chemistry. Nano Energy, 70, 104555.
58. Wen, Y., Rufford, T. E., Chen, X., Li, N., Lyu, M., Dai, L., & Wang, L. (2017). Nitrogen-doped Ti3C2Tx MXene electrodes for high-performance supercapacitors. Nano energy, 38, 368-376.
59. Li, J., Yan, D., Hou, S., Li, Y., Lu, T., Yao, Y., & Pan, L. (2018). Improved sodium-ion storage performance of Ti 3 C 2 T x MXenes by sulfur doping. Journal of Materials Chemistry A, 6(3), 1234-1243.
60. Sun, S., Xie, Z., Yan, Y., & Wu, S. (2019). Hybrid energy storage mechanisms for sulfur-decorated Ti3C2 MXene anode material for high-rate and long-life sodium-ion batteries. Chemical Engineering Journal, 366, 460-467.
61. Yoon, Y., Tiwari, A. P., Choi, M., Novak, T. G., Song, W., Chang, H., ... & An, K. S. (2019). Precious-metal-free electrocatalysts for activation of hydrogen evolution with nonmetallic electron donor: chemical composition controllable phosphorous doped vanadium carbide MXene. Advanced Functional Materials, 29(30), 1903443.
62. Liu, S., Hu, F., Shao, W., Zhang, W., Zhang, T., Song, C., ... & Jian, X. (2020). A novel strategy of in situ trimerization of cyano groups between the Ti 3 C 2 T x (MXene) interlayers for high-energy and high-power sodium-ion capacitors. Nano-Micro Letters, 12, 1-15.
63. Yang, C., Tang, Y., Tian, Y., Luo, Y., Faraz Ud Din, M., Yin, X., & Que, W. (2018). Flexible nitrogen-doped 2D titanium carbides (MXene) films constructed by an ex situ solvothermal method with extraordinary volumetric capacitance. Advanced Energy Materials, 8(31), 1802087.
64. Fan, Z., Wei, C., Yu, L., Xia, Z., Cai, J., Tian, Z., ... & Sun, J. (2020). 3D printing of porous nitrogen-doped Ti3C2 MXene scaffolds for high-performance sodium-ion hybrid capacitors. ACS nano, 14(1), 867-876.
65. Song, Y., Sun, Z., Fan, Z., Cai, W., Shao, Y., Sheng, G., ... & Sun, J. (2020). Rational design of porous nitrogen-doped Ti3C2 MXene as a multifunctional electrocatalyst for Li–S chemistry. Nano Energy, 70, 104555.
66. Yang, C., Tang, Y., Tian, Y., Luo, Y., Faraz Ud Din, M., Yin, X., & Que, W. (2018). Flexible nitrogen-doped 2D titanium carbides (MXene) films constructed by an ex situ solvothermal method with extraordinary volumetric capacitance. Advanced Energy Materials, 8(31), 1802087.
67. Sun, S., Xie, Z., Yan, Y., & Wu, S. (2019). Hybrid energy storage mechanisms for sulfur-decorated Ti3C2 MXene anode material for high-rate and long-life sodium-ion batteries. Chemical Engineering Journal, 366, 460-467.
68. Zhang, J., Zhao, Y., Guo, X., Chen, C., Dong, C. L., Liu, R. S., ... & Wang, G. (2018). Single platinum atoms immobilized on an MXene as an efficient catalyst for the hydrogen evolution reaction. Nature Catalysis, 1(12), 985-992.
69. Wang, Y., Gu, F., Cao, L., Fan, L., Hou, T., Zhu, Q., ... & Xiong, S. (2022). TiCN MXene hybrid BCN nanotubes with trace level Co as an efficient ORR electrocatalyst for Zn-air batteries. International Journal of Hydrogen Energy, 47(48), 20894-20904.
70. Yang, Q., Yang, T., Gao, W., Qi, Y., Guo, B., Zhong, W., ... & Xu, M. (2020). An MXene-based aerogel with cobalt nanoparticles as an efficient sulfur host for room-temperature Na–S batteries. Inorganic Chemistry Frontiers, 7(22), 4396-4403.
71. Lukatskaya, M. R., Mashtalir, O., Ren, C. E., Dall'Agnese, Y., Rozier, P., Taberna, P. L., ... & Gogotsi, Y. (2013). Cation intercalation and high volumetric capacitance of two-dimensional titanium carbide. Science, 341(6153), 1502-1505.
72. Li, J., Yuan, X., Lin, C., Yang, Y., Xu, L., Du, X., ... & Sun, J. (2017). Achieving high pseudocapacitance of 2D titanium carbide (MXene) by cation intercalation and surface modification. Advanced Energy Materials, 7(15), 1602725.

73. Mashtalir, O., Lukatskaya, M. R., Kolesnikov, A. I., Raymundo-Pinero, E., Naguib, M., Barsoum, M. W., & Gogotsi, Y. (2016). The effect of hydrazine intercalation on the structure and capacitance of 2D titanium carbide (MXene). Nanoscale, 8(17), 9128-9133.
74. Dillon, A. D., Ghidiu, M. J., Krick, A. L., Griggs, J., May, S. J., Gogotsi, Y., ... & Fafarman, A. T. (2016). Highly conductive optical quality solution-processed films of 2D titanium carbide. Advanced Functional Materials, 26(23), 4162-4168.
75. Sarycheva, A., Polemi, A., Liu, Y., Dandekar, K., Anasori, B., & Gogotsi, Y. (2018). 2D titanium carbide (MXene) for wireless communication. Science advances, 4(9), eaau0920.
76. Kim, S. J., Choi, J., Maleski, K., Hantanasirisakul, K., Jung, H. T., Gogotsi, Y., & Ahn, C. W. (2019). Interfacial assembly of ultrathin, functional MXene films. ACS applied materials & interfaces, 11(35), 32320-32327.
77. Huang, H., Cui, J., Liu, G., Bi, R., & Zhang, L. (2019). Carbon-coated MoSe2/MXene hybrid nanosheets for superior potassium storage. Acs Nano, 13(3), 3448-3456.
78. Zhang, X., Ni, Z., Bai, X., Shen, H., Wang, Z., Wei, C., ... & Feng, J. (2023). Hierarchical Porous N-doped Carbon Encapsulated Fluorine-free MXene with Tunable Coordination Chemistry by One-pot Etching Strategy for Lithium–Sulfur Batteries. Advanced Energy Materials, 13(29), 2301349.
79. Wang, H., He, S. A., Cui, Z., Xu, C., Zhu, J., Liu, Q., ... & Zou, R. (2021). Enhanced kinetics and efficient activation of sulfur by ultrathin MXene coating S-CNTs porous sphere for highly stable and fast charging lithium-sulfur batteries. Chemical Engineering Journal, 420, 129693.
80. Li, Y., Zhu, Q., Xu, M., Zang, B., Wang, Y., & Xu, B. (2023). Cu-Modified Ti3C2Cl2 MXene with Zincophilic and Hydrophobic Characteristics as a Protective Coating for Highly Stable Zn Anode. Advanced Functional Materials, 33(18), 2213416.
81. Ying, G., Dillon, A. D., Fafarman, A. T., & Barsoum, M. W. (2017). Transparent, conductive solution processed spincast 2d ti2ct x (mxene) films. Materials Research Letters, 5(6), 391-398.
82. Salles, P.; Quain, E.; Kurra, N.; Sarycheva, A.; Gogotsi, Y. Automated Scalpel Patterning of Solution Processed Thin Films for Fabrication of Transparent MXene Microsupercapacitors. Small 2018, 14, 1802864.
83. Kim, S. J., Choi, J., Maleski, K., Hantanasirisakul, K., Jung, H. T., Gogotsi, Y., & Ahn, C. W. (2019). Interfacial assembly of ultrathin, functional MXene films. ACS applied materials & interfaces, 11(35), 32320-32327.
84. Gao, L., Bao, W., Kuklin, A. V., Mei, S., Zhang, H., & Ågren, H. (2021). Hetero-MXenes: theory, synthesis, and emerging applications. Advanced Materials, 33(10), 2004129.
85. Zhang, J., Zhao, Y., Guo, X., Chen, C., Dong, C. L., Liu, R. S., ... & Wang, G. (2018). Single platinum atoms immobilized on an MXene as an efficient catalyst for the hydrogen evolution reaction. Nature Catalysis, 1(12), 985-992.
86. Xu, Q., Ding, L., Wen, Y., Yang, W., Zhou, H., Chen, X., ... & Li, N. (2018). High photoluminescence quantum yield of 18.7% by using nitrogen-doped Ti 3 C 2 MXene quantum dots. Journal of Materials Chemistry C, 6(24), 6360-6369.
87. Bao, W., Liu, L., Wang, C., Choi, S., Wang, D., & Wang, G. (2018). Facile synthesis of crumpled nitrogen-doped mxene nanosheets as a new sulfur host for lithium–sulfur batteries. Advanced Energy Materials, 8(13), 1702485.
88. Luo, J., Zheng, J., Nai, J., Jin, C., Yuan, H., Sheng, O., ... & Tao, X. (2019). Atomic sulfur covalently engineered interlayers of Ti3C2 MXene for ultra-fast sodium-ion storage by enhanced pseudocapacitance. Advanced Functional Materials, 29(10), 1808107.
89. Deng, Y., Shang, T., Wu, Z., Tao, Y., Luo, C., Liang, J., ... & Yang, Q. H. (2019). Fast gelation of Ti3C2Tx MXene initiated by metal ions. Advanced Materials, 31(43), 1902432.
90. Naguib, M., Mashtalir, O., Carle, J., Presser, V., Lu, J., Hultman, L., ... & Barsoum, M. W. (2012). Two-dimensional transition metal carbides. ACS nano, 6(2), 1322-1331.
91. Yang, C., Tang, Y., Tian, Y., Luo, Y., Faraz Ud Din, M., Yin, X., & Que, W. (2018). Flexible nitrogen-doped 2D titanium carbides (MXene) films constructed by an ex situ solvothermal method with extraordinary volumetric capacitance. Advanced Energy Materials, 8(31), 1802087.
92. Tang, Y., Yang, C., Tian, Y., Luo, Y., Yin, X., & Que, W. (2020). The effect of in situ nitrogen doping on the oxygen evolution reaction of MXenes. Nanoscale Advances, 2(3), 1187-1194.
93. Bilibana, M. P. (2023). Electrochemical Properties of MXenes and Applications. Advanced Sensor and Energy Materials, 100080.
94. Ampong, D. N., Agyekum, E., Agyemang, F. O., Mensah-Darkwa, K., Andrews, A., Kumar, A., & Gupta, R. K. (2023). MXene: fundamentals to applications in electrochemical energy storage. Discover Nano, 18(1), 3.
95. Ma, P., Fang, D., Liu, Y., Shang, Y., Shi, Y., & Yang, H. Y. (2021). MXene-based materials for electrochemical sodium-ion storage. Advanced Science, 8(11), 2003185.
96. Ma, G., Shao, H., Xu, J., Liu, Y., Huang, Q., Taberna, P. L., ... & Lin, Z. (2021). Li-ion storage properties of two-dimensional titanium-carbide synthesized via fast one-pot method in air atmosphere. Nature communications, 12(1), 5085.
97. Zhao, Q., Zhu, Q., Liu, Y., & Xu, B. (2021). Status and prospects of MXene-based lithium–sulfur batteries. Advanced Functional Materials, 31(21), 2100457.
98. Junaidi, N. H. A., Wong, W. Y., Loh, K. S., Rahman, S., Choo, T. F., & Wu, B. (2023). Enhanced oxygen reduction reaction catalyst stability and durability of MXene-supported Fe-NC catalyst for proton exchange membrane fuel cell application. Journal of Alloys and Compounds, 968, 171898.
99. Xiao, J., Wu, B., Bai, L., Ma, X., Lu, H., Yao, J., ... & Gao, H. (2022). Ag Nanoparticles decorated few-layer Nb2CTx nanosheets architectures with superior lithium/sodium-ion storage. Electrochimica Acta, 402, 139566.
100. Liu, Y. T., Zhang, P., Sun, N., Anasori, B., Zhu, Q. Z., Liu, H., ... & Xu, B. (2018). Self-assembly of transition metal oxide nanostructures on MXene nanosheets for fast and stable lithium storage. Advanced Materials, 30(23), 1707334.
101. Deng, Y., Shang, T., Wu, Z., Tao, Y., Luo, C., Liang, J., ... & Yang, Q. H. (2019). Fast gelation of Ti3C2Tx MXene initiated by metal ions. Advanced Materials, 31(43), 1902432.

102. Yu, L., Fan, Z., Shao, Y., Tian, Z., Sun, J., & Liu, Z. (2019). Versatile N-doped MXene ink for printed electrochemical energy storage application. Advanced Energy Materials, 9(34), 1901839.
103. Li, Y., Chen, X., Sun, Y., Meng, X., Dall'Agnese, Y., Chen, G., ... & Ren, H. (2020). S. Sasaki, H. Tamiaki, X.-F. Wang. Adv. Mater. Interfaces, 7, 1902080.
104. Liu, R., Cao, W., Han, D., Mo, Y., Zeng, H., Yang, H., & Li, W. (2019). Nitrogen-doped Nb2CTx MXene as anode materials for lithium ion batteries. Journal of Alloys and Compounds, 793, 505-511.
105. Wang, C., Xie, H., Chen, S., Ge, B., Liu, D., Wu, C., ... & Song, L. (2018). Atomic cobalt covalently engineered interlayers for superior lithium-ion storage. Advanced Materials, 30(32), 1802525.
106. Huang, W., Zhang, Y., You, Q., Huang, P., Wang, Y., Huang, Z. N., ... & Zhang, H. (2019). Enhanced photodetection properties of tellurium@ selenium roll-to-roll nanotube heterojunctions. Small, 15(23), 1900902.
107. Li, Q., Zhu, H., Tang, Y., Zhu, P., Ma, H., Ge, C., & Yan, F. (2019). Chemically grafting nanoscale UIO-66 onto polypyrrole nanotubes for long-life lithium–sulfur batteries. Chemical communications, 55(80), 12108-12111.
108. Xiao, R., Zhao, C., Zou, Z., Chen, Z., Tian, L., Xu, H., ... & Yang, X. (2020). In situ fabrication of 1D CdS nanorod/2D Ti3C2 MXene nanosheet Schottky heterojunction toward enhanced photocatalytic hydrogen evolution. Applied Catalysis B: Environmental, 268, 118382.
109. Lin, J., Yu, Y., Zhang, Z., Gao, F., Liu, S., Wang, W., & Li, G. (2020). A novel approach for achieving high-efficiency photoelectrochemical water oxidation in InGaN nanorods grown on Si system: Mxene nanosheets as multifunctional interfacial modifier. Advanced Functional Materials, 30(13), 1910479.
110. Zhao, M. Q., Ren, C. E., Ling, Z., Lukatskaya, M. R., Zhang, C., Van Aken, K. L., ... & Gogotsi, Y. (2014). Flexible MXene/carbon nanotube composite paper with high volumetric capacitance. Advanced materials, 27(2).
111. Wang, J., Zhang, Z., Yan, X., Zhang, S., Wu, Z., Zhuang, Z., & Han, W. Q. (2020). Rational design of porous N-Ti 3 C 2 MXene@ CNT microspheres for high cycling stability in Li–S battery. Nano-Micro Letters, 12, 1-14.
112. Zhang, P., Zhu, Q., Soomro, R. A., He, S., Sun, N., Qiao, N., & Xu, B. (2020). In situ ice template approach to fabricate 3D flexible MXene film-based electrode for high performance supercapacitors. Advanced Functional Materials, 30(47), 2000922.
113. Cui, C., Guo, R., Xiao, H., Ren, E., Song, Q., Xiang, C., ... & Jiang, S. (2020). Bi2WO6/Nb2CTx MXene hybrid nanosheets with enhanced visible-light-driven photocatalytic activity for organic pollutants degradation. Applied Surface Science, 505, 144595.
114. Yue, Y., Liu, N., Ma, Y., Wang, S., Liu, W., Luo, C., ... & Gao, Y. (2018). Highly self-healable 3D microsupercapacitor with MXene–graphene composite aerogel. Acs Nano, 12(5), 4224-4232.
115. Xiu LY, Wang ZY, Yu MZ, Wu XH, Qiu JS. Aggregationresistant 3D MXene-based architecture as efficient bifunctional electrocatalyst for overall water splitting. ACS Nano. 2018;12 (8):8017-8028.
116. Zhao, M. Q., Xie, X., Ren, C. E., Makaryan, T., Anasori, B., Wang, G., & Gogotsi, Y. (2017). Hollow MXene spheres and 3D macroporous MXene frameworks for Na-ion storage. Advanced materials, 29(37), 1702410.
117. Shang, T., Lin, Z., Qi, C., Liu, X., Li, P., Tao, Y., ... & Yang, Q. H. (2019). 3D macroscopic architectures from self-assembled MXene hydrogels. Advanced Functional Materials, 29(33), 1903960.
118. Bao, W., Liu, L., Wang, C., Choi, S., Wang, D., & Wang, G. (2018). Facile synthesis of crumpled nitrogen-doped mxene nanosheets as a new sulfur host for lithium–sulfur batteries. Advanced Energy Materials, 8(13), 1702485.
119. Shang, T., Lin, Z., Qi, C., Liu, X., Li, P., Tao, Y., ... & Yang, Q. H. (2019). 3D macroscopic architectures from self-assembled MXene hydrogels. Advanced Functional Materials, 29(33), 1903960.
120. Luo, J., Matios, E., Wang, H., Tao, X., & Li, W. (2020). Interfacial structure design of MXene-based nanomaterials for electrochemical energy storage and conversion. InfoMat, 2(6), 1057-1076.
121. Luo, J., Zheng, J., Nai, J., Jin, C., Yuan, H., Sheng, O., ... & Tao, X. (2019). Atomic sulfur covalently engineered interlayers of Ti3C2 MXene for ultra-fast sodium-ion storage by enhanced pseudocapacitance. Advanced Functional Materials, 29(10), 1808107.
122. Luo J, Tao X, Zhang J, et al. Sn4+ ion decorated highly conduc tive Ti3C2 MXene: promising lithium-ion anodes with enhanced volumetric capacity and cyclic performance. ACS Nano. 2016;10(2):2491-2499.
123. Luo JM, Wang CL, Wang H, et al. Pillared MXene with ultralarge interlayer spacing as a stable matrix for high performance sodium metal anodes. Adv Funct Mater. 2019;29(3):1805946.
124. Yan, J., Ren, C. E., Maleski, K., Hatter, C. B., Anasori, B., Urbankowski, P., ... & Gogotsi, Y. (2017). Flexible MXene/graphene films for ultrafast supercapacitors with outstanding volumetric capacitance. Advanced Functional Materials, 27(30), 1701264.
125. Chen, C., Xie, X., Anasori, B., Sarycheva, A., Makaryan, T., Zhao, M., ... & Gogotsi, Y. (2018). MoS2-on-MXene heterostructures as highly reversible anode materials for lithium-ion batteries. Angewandte Chemie International Edition, 57(7), 1846-1850.
126. Ahmed, B., Anjum, D. H., Gogotsi, Y., & Alshareef, H. N. (2017). Atomic layer deposition of SnO2 on MXene for Li-ion battery anodes. Nano Energy, 34, 249-256.
127. Rakhi, R. B., Ahmed, B., Hedhili, M. N., Anjum, D. H., & Alshareef, H. N. (2015). Effect of postetch annealing gas composition on the structural and electrochemical properties of Ti2CT x MXene electrodes for supercapacitor applications. Chemistry of Materials, 27(15), 5314-5323.
128. Zou, Z., Wang, Q., Yan, J., Zhu, K., Ye, K., Wang, G., & Cao, D. (2021). Versatile interfacial self-assembly of Ti3C2T x MXene based composites with enhanced kinetics for superior lithium and sodium storage. ACS nano, 15(7), 12140-12150.
129. Yao, L., Liang, F., Jin, J., Chowdari, B. V., Yang, J., & Wen, Z. (2020). Improved electrochemical property of Ni-rich LiNi0. 6Co0. 2Mn0. 2O2 cathode via in-situ ZrO2 coating for high energy density lithium ion batteries. Chemical engineering journal, 389, 124403.
130. Sha, D., Lu, C., He, W., Ding, J., Zhang, H., Bao, Z., ... & Sun, Z. (2022). Surface Selenization Strategy for V2CT x MXene toward Superior Zn-Ion Storage. ACS nano, 16(2), 2711-2720.

131. Li, H., Li, J., Ma, L., Zhang, X., Li, J., Li, J., ... & Pan, L. (2023). Heteroatomic interface engineering of an octahedron VSe 2–ZrO 2/C/MXene composite derived from a MXene-MOF hybrid as a superior-performance anode for lithium-ion batteries. Journal of Materials Chemistry A, 11(6), 2836-2847.
132. Wang, X., Wang, J., Qin, J., Xie, X., Yang, R., & Cao, M. (2020). Surface charge engineering for covalently assembling three-dimensional MXene network for all-climate sodium ion batteries. ACS applied materials & interfaces, 12(35), 39181-39194.
133. Ji, J., Zhao, L., Shen, Y., Liu, S., & Zhang, Y. (2019). Covalent stabilization and functionalization of MXene via silylation reactions with improved surface properties. FlatChem, 17, 100128.
134. Kim, J., Yoon, Y., Kim, S. K., Park, S., Song, W., Myung, S., ... & An, K. S. (2021). Chemically stabilized and functionalized 2D-MXene with deep eutectic solvents as versatile dispersion medium. Advanced Functional Materials, 31(13), 2008722.
135. Zhao, Y., Li, Q., Liu, Z., Fan, L., Li, J., Ma, Z., ... & Shao, G. (2020). Stable electrochemical Li plating/stripping behavior by anchoring MXene layers on three-dimensional conductive skeletons. ACS applied materials & interfaces, 12(34), 37967-37976.
136. Sun, C., Wu, C., Gu, X., Wang, C., & Wang, Q. (2021). Interface engineering via Ti 3 C 2 T x MXene electrolyte additive toward dendrite-free zinc deposition. Nano-micro letters, 13, 1-13.
137. Cao, Z., Zhuang, P., Zhang, X., Ye, M., Shen, J., & Ajayan, P. M. (2020). Strategies for dendrite-free anode in aqueous rechargeable zinc ion batteries. Advanced Energy Materials, 10(30), 2001599.
138. Qiao, H., Zhu, X., Li, X., Wang, Y., Ye, C., Ma, L., ... & Ye, M. (2024). Uncovering Synergistic Effects of Electrode/Electrolyte Toward Concerted Cathodic Structure Stabilization for Superior-Performance Aqueous Zn-δ-MnO2 Battery. Advanced Energy Materials, 14(18), 2304357.
139. Okubo, M., Sugahara, A., Kajiyama, S., & Yamada, A. (2018). MXene as a charge storage host. Accounts of chemical research, 51(3), 591-599.
140. Nan, J., Guo, X., Xiao, J., Li, X., Chen, W., Wu, W., ... & Wang, G. (2021). Nanoengineering of 2D MXene-based materials for energy storage applications. Small, 17(9), 1902085.
141. Bergman, G., Ballas, E., Gao, Q., Nimkar, A., Gavriel, B., Levi, M. D., ... & Aurbach, D. (2023). Elucidation of the Charging Mechanisms and the Coupled Structural–Mechanical Behavior of Ti3C2Tx (MXenes) Electrodes by In Situ Techniques. Advanced Energy Materials, 13(8), 2203154.
142. Das, M., & Ghosh, S. (2024). Improved charge storage capacity of supercapacitor electrodes by engineering surfaces: the case of Janus MXenes. The Journal of Physical Chemistry C, 128(3), 1014-1023.
143. Naguib, M., Halim, J., Lu, J., Cook, K. M., Hultman, L., Gogotsi, Y., & Barsoum, M. W. (2013). New two-dimensional niobium and vanadium carbides as promising materials for Li-ion batteries. Journal of the American Chemical Society, 135(43), 15966-15969.
144. Wang, H., Wu, Y., Yuan, X., Zeng, G., Zhou, J., Wang, X., & Chew, J. W. (2018). Clay-inspired MXene-based electrochemical devices and photo-electrocatalyst: state-of-the-art progresses and challenges. Advanced Materials, 30(12), 1704561.
145. Dall'Agnese, Y., Lukatskaya, M. R., Cook, K. M., Taberna, P. L., Gogotsi, Y., & Simon, P. (2014). High capacitance of surface-modified 2D titanium carbide in acidic electrolyte. Electrochemistry Communications, 48, 118-122.
146. Maleski, K., Mochalin, V. N., & Gogotsi, Y. (2017). Dispersions of two-dimensional titanium carbide MXene in organic solvents. Chemistry of Materials, 29(4), 1632-1640.
147. Hart, J. L., Hantanasirisakul, K., Lang, A. C., Anasori, B., Pinto, D., Pivak, Y., ... & Taheri, M. L. (2019). Control of MXenes' electronic properties through termination and intercalation. Nature communications, 10(1), 522.
148. An, H., Habib, T., Shah, S., Gao, H., Radovic, M., Green, M. J., & Lutkenhaus, J. L. (2018). Surface-agnostic highly stretchable and bendable conductive MXene multilayers. Science advances, 4(3), eaaq0118.
149. Ansari, M. Z., Seo, K. M., Kim, S. H., & Ansari, S. A. (2022). Critical aspects of various techniques for synthesizing metal oxides and fabricating their composite-based supercapacitor electrodes: a review. Nanomaterials, 12(11), 1873.
150. Zhang, C., McKeon, L., Kremer, M. P., Park, S. H., Ronan, O., Seral-Ascaso, A., ... & Nicolosi, V. (2019). Additive-free MXene inks and direct printing of micro-supercapacitors. Nature communications, 10(1), 1795.
151. Zhan, C., Naguib, M., Lukatskaya, M., Kent, P. R., Gogotsi, Y., & Jiang, D. E. (2018). Understanding the MXene pseudocapacitance. The journal of physical chemistry letters, 9(6), 1223-1228.
152. Hussain, I., Lamiel, C., Javed, M. S., Ahmad, M., Chen, X., Sahoo, S., ... & Zhang, K. (2023). Earth-and marine-life-resembling nanostructures for electrochemical energy storage. Chemical Engineering Journal, 454, 140313.
153. Simon, P. (2017). Two-dimensional MXene with controlled interlayer spacing for electrochemical energy storage. ACS nano, 11(3), 2393-2396.
154. Li, J., Guo, C., & Li, C. M. (2020). Recent Advances of Two-Dimensional (2 D) MXenes and Phosphorene for High-Performance Rechargeable Batteries. ChemSusChem, 13(6), 1047-1070.
155. Naguib, M., Mochalin, V. N., Barsoum, M. W., & Gogotsi, Y. (2014). 25th anniversary article: MXenes: a new family of two-dimensional materials. Advanced materials, 26(7), 992-1005.